



POLYTECHNIC UNIVERSITY OF BARI

Master's degree in MECHANICAL ENGINEERING

Department of MECHANICS, MATHEMATICS AND MANAGEMENT

MICROFLUIDIC DEVICES FOR MEDICAL APPLICATIONS

by

Angelantonio SQUICCIARINI

Supervisor:

Prof. Eng. Marco Donato DE TULLIO

Marco Donato de Tullio
Co-Supervisors:

Dr. Dario DE MARINIS

Dr. Francesco FERRARA

Academic Year 2021/2022



**LIBERATORIA ALLA CONSULTAZIONE DELLA TESI DI LAUREA DI CUI
ALL'ART.4 DEL REGOLAMENTO DI ATENEO PER LA CONSULTAZIONE DELLE
TESI DI LAUREA (D.R. n. 479 del 14/11/2016).**

Il sottoscritto SQUICCIARINI ANGELANTONIO matricola 583472

Corso di Laurea LM-33 MECHANICAL ENGINEERING

autore della presente tesi di Laurea dal titolo MICROFLUIDIC DEVICES FOR MEDICAL APPLICATIONS

Parola chiave MICROFLUIDIC DEVICES

Abstract SIMULAZIONE FLUIDODINAMICA ATTRAVERSO ANSYS FLUENT PER LA FOCALIZZAZIONE CELLULARE DI LINFOCITI T DISPERSI IN SOLUZIONE ACQUOSA. IMPLEMENTAZIONE DI UNA UDF PER INCLUDERE FORZE RILEVANTI NELLA MICROFLUIDICA CHE CONSENTONO IL FOCUSING CELLULARE.

Autorizza

Non autorizza

la consultazione della presente tesi, fatto divieto a chiunque di riprodurre in tutto o in parte quanto in essa contenuto.

Bari,

Firma

Angelantonio Squicciarini

Contents

0.1	INTRODUCTION	4
1	COMPOSITION OF BLOOD AND ITS FUNCTIONS	5
1.1	Leukocytes and blood composition	5
1.2	CAR-T therapy	7
2	MICROFLUIDIC APPLICATION IN CELL SEPARATION	9
2.1	Viscous drag force	9
2.2	Magnus force–rotation-induced lift force	10
2.3	Saffman lift force	11
2.4	Wall-induced lift force	12
2.5	Shear gradient lift force	12
2.6	Net inertial lift force	13
2.7	Dean Flow Drag Force	14
2.8	Cross Section	18
2.9	Comparison between trapezoidal and rectangular cross sections	20
2.10	The effect of inward and outward slopping of trapezoid cross section	22
2.11	Straight Channel Length	22
2.12	Serpentine Micro channel	23
2.13	Distance between particles	25
3	DPM IN ANSYS FLUENT	27
3.1	Introduction	27
3.2	Particle Motion Theory	27
4	ANSYS FLUENT SIMULATION	33
4.1	Test spiral micro channel to capture Dean vortices	33
4.2	Experiment particle/parcels	35
4.3	Simulation of spiral micro channel	37
4.3.1	Single injection	41
4.3.2	Surface injection	43

5 UDF IMPLEMENTATION AND FINAL RESULTS	46
5.1 Numerical method for lift force	46
5.2 Simple straight channel test	46
5.3 Particles focusing in a straight channel	51
5.4 General UDF for different channel shape	52
5.5 Results of spiral channel with rectangular cross section	55
5.6 Improvement of the model	56
5.7 Simulation of 3 loops spiral channel with AR=0.5, Re=100 and k=0.1	59
5.8 Simulation of 3 loops spiral channel with AR=0.5, Re=50 and k=0.1	65
6 FABRICATION OF THE SPIRAL CHANNEL	67
7 EXPERIMENT SET UP AND FINAL RESULTS	71
7.1 Elveflow controller	71
7.2 Injection of particles into the spiral and results	72
8 CONCLUSIONS	74
Bibliography	76
A	78
B	82

0.1 INTRODUCTION

This thesis has been realized in collaboration with CNR NANOTEC Lecce and ST MICROELECTRONICS - Lecce.

The work of this thesis has been originated in the context of the ongoing TITAN (Tumor ImmunoTherapy by Nanotechnology) project, with the aim of designing a microfluidic device where inertial effects can be exploited to generate secondary flows and particle migration, so that desired particle focusing can be achieved without the need for external forces acting on the system. In this way, cells are aligned and can be counted by a sensor placed downstream the device.

A curved microchannel with spiral geometry has been selected as design solution. The spiral geometry has been drawn by using INVENTOR and the obtained CAD file has been imported in POINTWISE where mesh generation and optimization has been performed.

Computational Fluid Dynamics simulations has been performed by using ANSYS FLUENT software. The microfluidic effects on the transport of particles suspended within the fluid phase have been modelled and the model has been included in the basic ANSYS FLUENT software by means of a user-defined function (UDF).

After the preliminar numerical validation, the optimized geometry of the spiral has been fabricated, using CNC micro-mill working on a G-code obtained by FUSION360 software.

Finally, the device has been tested experimentally and results has been obtained by using the ELVEFLOW controller coupled with a fluorescence microscope.

Chapter 1

COMPOSITION OF BLOOD AND ITS FUNCTIONS

1.1 Leukocytes and blood composition

The cellular portion of blood is composed of plasma, leukocytes or white blood cells (WBC) and red blood cells (RBC) containing hemoglobin which carries oxygen and carbon dioxide in the body, as can be seen in Figure 1.1.

WBC are blood cells involved in the immune response. Thanks to their immunological action, the body defends itself against pathogenic microorganisms (such as viruses, bacteria, fungi and parasites), foreign particles and potentially harmful abnormal cells present within the blood and tissues. Mature leukocytes circulating in the blood include very different cell populations (neutrophils, eosinophils, basophils, lymphocytes, monocytes), each performing specific functions in immune processes.

STRUCTURE OF BLOOD

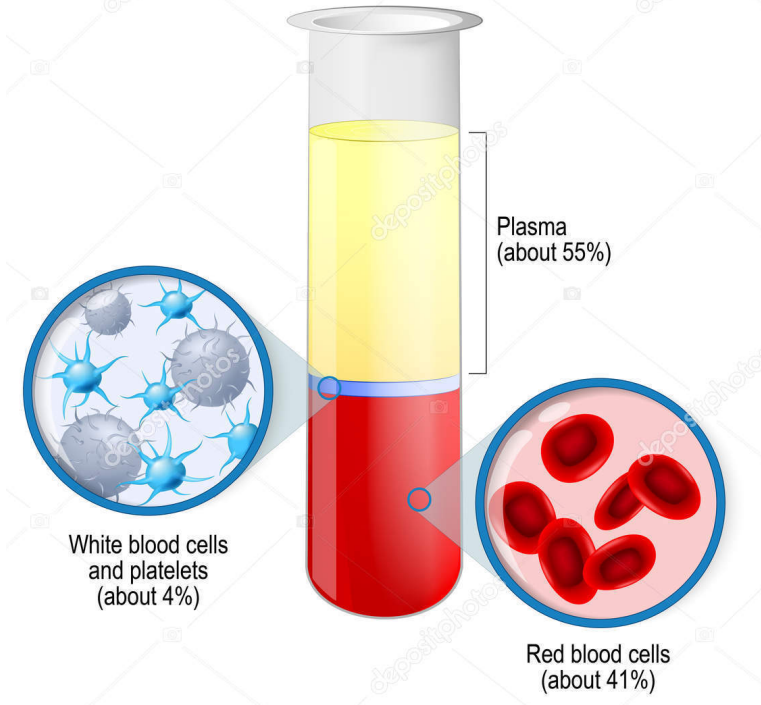


Figure 1.1: structure of blood

The separation of these three phases can be obtained by using a centrifugal machine.

Leukocytes, as well as other circulating blood cells, originate from precursors present in the bone marrow, a soft and "spongy" tissue, which is present in the hollow interior of the bones (vertebrae, ribs, pelvis, skull and epiphysis of the long bones).

Based on the morphological characteristics and the different affinity towards some histological dyes, five types of white blood cells can be grouped into two families - that of granulocytes and that of agranulocytes - depending on the presence or absence of granules in the cytoplasm. Granulocytes are further divided into basophils, neutrophils and eosinophils, while agranulocytes include monocytes and lymphocytes (the latter further divided into several subtypes, being T, B and Natural Killer or NK lymphocytes the most important among them), Figure 1.2.

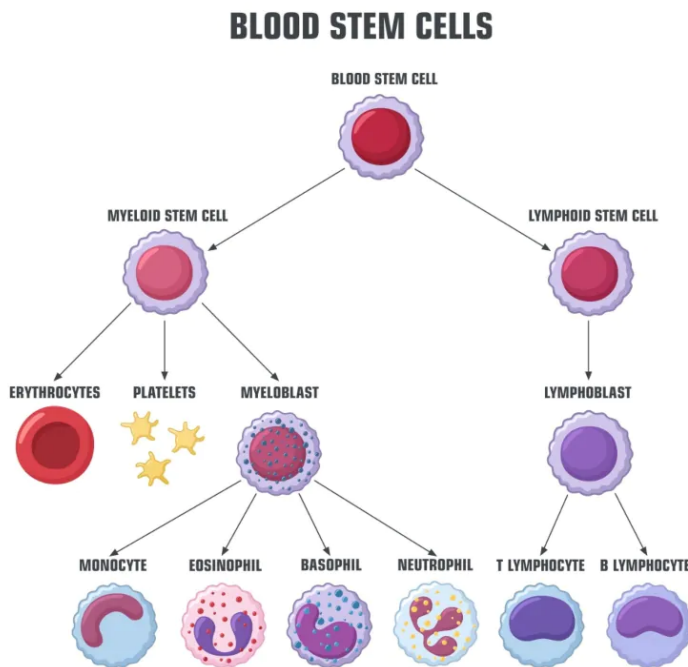


Figure 1.2: types of white blood cells

The size of Lymphocytes is about $5\text{-}17 \mu\text{m}$ and the morphological characteristics are: large core, little cytoplasm and absence of granules.

T lymphocytes: They induce a cell-mediated response, i.e. they are able to specifically recognize "self" antigens from "non-self" antigens;

They process molecules that are important in the defense against infections, that is, they produce cytokines that support the immune response and factors that destroy infected or neoplastic cells;

They initiate and control the extent of the immune response, increasing it as needed and slowing it down when the problem is resolved;

They play an essential role in transplant rejection.

Plasma cells (fully mature forms of B cells) produce antibody directed against bacteria, viruses and other "non-self" foreign antigens and destroy them.

T-helper lymphocytes produce cytokines that activate different cell types, amplifying the immune response;

Cytotoxic T cells attack infected or tumor cells and induce their lysis;

Natural Killer lymphocytes (NK cells) produce factors that induce the death (apoptosis) of cells recognized as infected and are able to kill some cancer cells.

1.2 CAR-T therapy

The "CAR-T" (Chimeric Antigen Receptor T cell) therapies are innovative personalized immunotherapies against cancer that acts directly on the patient's immune system to make it able to recognize

and destroy cancer cells.

CAR-Ts use specific immune cells (T lymphocytes), which are extracted from a blood sample of the patient; the T lymphocytes are then genetically modified and grown in the laboratory ("engineered") to be re-infused into the patient to induce a systemic response against autoimmune or cancer diseases. They are therefore distinguished from other known immune therapies such as "Immunological checkpoint inhibitors" (e.g. monoclonals antibodies), which target proteins working "as a brake" on the immune response, orienting it against cancer.

CAR-T therapy has so far proved effective for some hematological cancers, although trials for other therapeutic indications are in progress worldwide.

A CAR-T therapy requires a complex manufacturing procedure, which involves professionals and is divided into several phases:

1. **Collection:** T cells are collected from the blood at an authorized blood transfusion center, through a process that allows T cells isolation from peripheral blood (leukapheresis), and the reinjection of the remaining blood elements back into circulation. T lymphocytes are subsequently frozen and inserted into the structure that will take care of the engineering genetics modification.
2. **Genetic engineering:** the T lymphocytes are genetically modified, in highly qualified facilities for the production of advanced therapies. Using an inactivated virus (viral vector), a recombinant gene is added to the lymphocyte DNA carrying the code for a protein, known as a receptor, to be expressed on the surface of T lymphocytes of the Chemical Antigen (CAR). By integrating the code in the T cell genome and expressing this receptor, modified T lymphocytes (CAR-T cells) are able to recognize a specific antigen present on the surface of the cancer cells and bind to them, thus exerting their anti-tumoral activity. CAR-T cells multiply in a bioreactor under highly specific and controlled conditions, then they are frozen and sent to the healthcare center to be used as treatment.
3. **Pre-treatment chemotherapy (lymphodepleting):** before the infusion, the patient usually receive preparative chemotherapy to decreases the number of circulating T cells in order to allow new modified T lymphocytes to expand and activate in the body.
4. **Infusion:** after chemotherapy, CAR-T cells are infused into the patient, with a procedure similar to a blood transfusion. The infusion takes place in specialized clinic laboratories for the treatment of leukemias and lymphomas, with availability of access to intensive care.
5. **Monitoring:** after the infusion, hospitalisation is required for a few days and the patient is constantly monitored for adverse reactions to treatment. In the four weeks after discharge, the patient must live close to a qualified clinic for regular checks.

Chapter 2

MICROFLUIDIC APPLICATION IN CELL SEPARATION

In the past, most researchers believed that microfluidic devices should operate under laminar flow as well as Stokes flow ($Re \ll 1$) where particles flow in highly predictable streamlines. Moreover, in Stokes flow, inertial forces are small compared to viscous forces, so that forces evaluation is easier to be performed. We can define the Reynolds number (Re) as follows:

$$Re = \frac{\text{inertial force}}{\text{viscous force}} = \frac{\rho v_m D}{\mu} \quad (2.1)$$

where ρ is the fluid density, D is the characteristic length, v_m is the averaged velocity of the fluid and μ is the dynamic viscosity of the fluid.

However, in the regime of Reynolds number between 1 and 100, inertia can be exploited to generate particle migration and secondary flow effects.

Particles moving in such configurations migrate laterally to different equilibrium positions due to the counteraction of two inertial effects:

the shear gradient lift force due to the curvature of the fluid velocity profile, and the wall lift force as result of the interaction with the adjacent walls.

Secondary flow can also appear in curved channels, where the pressure gradient in the radial direction can generate two counter-rotating Dean vortices. This additional force on particles brings several advantages, changing the equilibrium position and allowing differential particle size-dependent focusing, depending on the ratio of inertial lift force to the secondary flow resistance [1].

2.1 Viscous drag force

Drag force arises when an object moves through a fluid or vice versa.. The drag force on a moving spherical particle can be expressed as:

$$F_{drag} = \frac{\pi a^2}{4} f_{drag} \quad (2.2)$$

Where a is the diameter of particle. f_{drag} is viscous drag coefficient which is always determined by the particle Reynolds number [2]:

$$Re' = \frac{v_t \rho_f a}{\mu} \quad (2.3)$$

v_t is the relative velocity between fluid and particle, μ is the dynamic viscosity of the fluid and ρ_f is the density of the fluid.

The viscous drag coefficient f_{drag} can be calculated in different ways depending on the particle Reynolds number Re' range [2]:

1) $10^{-4} < Re' < 0.2$

$$f_{drag} = 12 \frac{\mu v_t}{a} \quad (2.4)$$

$$F_{drag} = 3\pi \mu a v_t \quad (2.5)$$

This is the Stokes drag force.

2) $0.2 < Re' < 500 \sim 1000$

$$f_{drag} = 12\mu v_t a (1 + 0.15 Re'^{0.687}) \quad (2.6)$$

$$F_{drag} = 3\pi \mu v_t a (1 + 0.15 Re'^{0.687}) \quad (2.7)$$

3) $500 \sim 1000 < Re' < 2 \cdot 10^{-5}$

$$f_{drag} = 0.22 \rho_f v_t^2 \quad (2.8)$$

$$F_{drag} = 0.055 \pi a^2 \rho_f v_t^2 \quad (2.9)$$

2.2 Magnus force—rotation-induced lift force

In Figure 2.1 it is shown a cylinder immersed in an in-viscous flow with uniform velocity \vec{U} , that rotates with a certain constant angular velocity $\vec{\Omega}$ in clockwise direction.

It is known from Bernoulli equation that since the velocity at top part of the cylinder is higher than the bottom, it creates a difference of pressure that causes a lift force F_{LR} acting on the cylinder directed upward. The force for unit length of cylinder is [3]:

$$\vec{F}_{LR} = \pi \rho_f^2 a \vec{U} \times \vec{\Omega} \quad (2.10)$$

Considering the particle immersed in the fluid as a sphere, the lift force takes this form and is called Magnus force [4]:

$$\vec{F}_{LR} = \frac{1}{8}\pi a^3 \rho_f \vec{U} \times \vec{\Omega} \quad (2.11)$$

If the sphere also moves with a certain velocity \vec{u}_p , the Magnus force can be written using the relative velocity of the sphere with respect to the fluid:

$$\vec{F}_{LR} = \frac{1}{8}\pi a^3 \rho_f (\vec{u}_f - \vec{u}_p) \times \vec{\Omega} \quad (2.12)$$

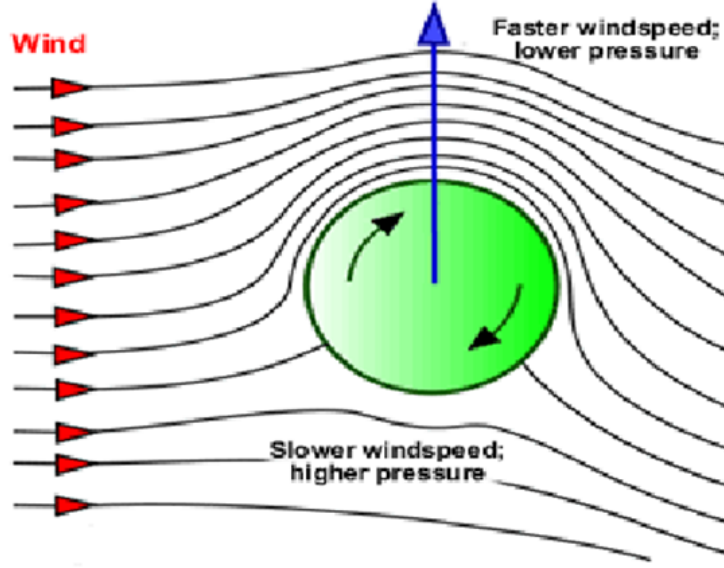


Figure 2.1: Magnus force

The above equations were derived for low Reynolds flows, Magnus forces also exist in high inertia flows. The Magnus force does not appear in creeping flows ($Re \ll 1$) but appears in all rotating viscous and inviscid fluid flows with a finite relative velocity.

2.3 Saffman lift force

The presence of the wall in a channel causes the parabolic profile of the velocity and so there is a gradient in the velocity profile (shear rate) that causes a lift force directed from the wall to the center of the channel. This force is called Saffman force. The Saffman force increases with the increasing of the relative velocity and also depends on particle size. The equation is:

$$F_S = \frac{K}{4} V_t a^2 (\gamma \nu^{-1})^{1/2} \quad (2.13)$$

where V_t is the relative velocity between particle and fluid, K is a numerical constant ($\sim 81, 2$), γ is the shear rate and ν is the kinetic viscosity.

2.4 Wall-induced lift force

The second effect of the wall can be seen when the particle stays close to the wall. When the particle moves close to the wall (vertically), a layer of liquid remains between the particle and the wall and this creates a drag, a pressure force acting on the particle toward the centre of the channel appears.

2.5 Shear gradient lift force

In Figure 2.2 it is shown a flow with a constant velocity that impacts a particle.

A control volume in red, that surround the particle is taken, and as can be seen, there is a certain surface S_0 where the velocity U is entering (so there is a certain flow ($Q = S_0 \cdot U$)).

The mass must be conserved and so the fluid will pass through the surface S_1 that is smaller than S_0 because the particle is there. Since the surface is lower, the velocity must increase, $U_1 > U$. Considering an in-viscid fluid, from Bernoulli equation the pressure $p_1 < p_0$. In this case there is no pressure force in vertical direction. It can be seen that the problem is symmetric.

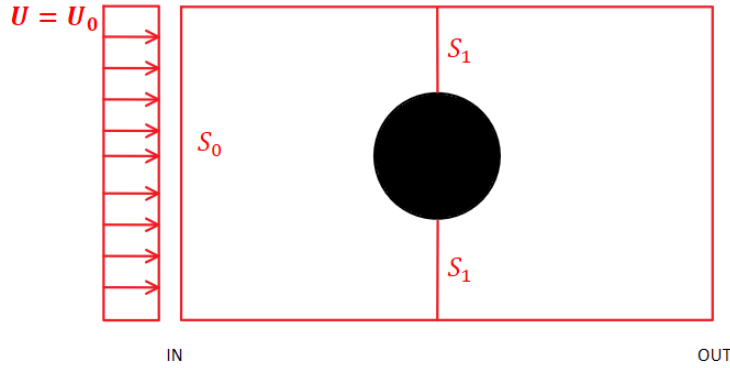


Figure 2.2: No shear gradient lift force

In Figure 2.3, since the wall is present, the velocity is not constant but parabolic. The attention was focused only in one half of the channel.

In this case, there is a gradient of velocity that is linear because the velocity profile is parabolic and so the particles move when the gradient is low and towards the wall (in Figure 2.3 the force is acting down). For parabolic flow, there is a shear rate that is linear and a shear gradient that is constant.

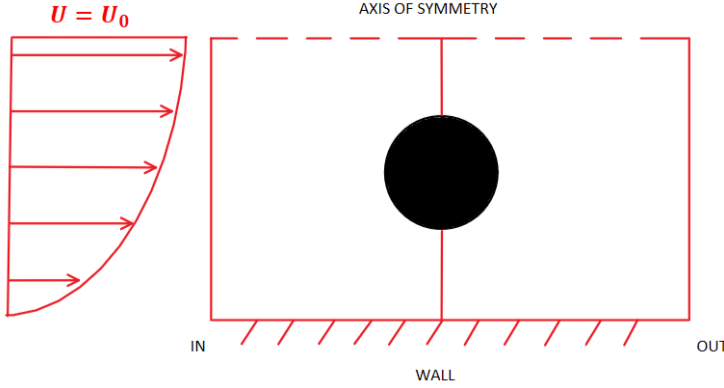


Figure 2.3: shear gradient lift force

2.6 Net inertial lift force

Magnus and Saffman forces are negligible in our configurations. Only the wall lift force and the shear gradient lift force are taken into account.

Asmolov [5] derived an analytical expression of the net inertial lift force acting on a small rigid sphere ($\frac{a}{D_h} \ll 1$) in a Poiseuille flow:

$$F_L = f_L \rho_f \gamma^2 a^4 \quad (2.14)$$

$$F_L = f_L \rho_f U^2 a^4 / D_h^2 \quad (2.15)$$

where D_h is the hydraulic diameter that for the circular section it coincides with diameter D , instead for the rectangular section it is $D_h = \frac{2HW}{H+W}$.

H and W are the height and the width of the cross section, respectively.

The lift coefficient f_L is a function of the lateral position X of the particle calculated with respect to the axis of the channel and on the Re [5]. Increasing Re the lift coefficient decreases. Zhou and Papautsky [6] derived a scaling for the lift coefficient based on their experimental results:

$$f_L \propto \frac{D_h^2}{a^2 \sqrt{Re}} \quad (2.16)$$

at $Re < 100$ the lift coefficient remains constant, and can be approximated averagely as $f_L = 0.5$ [8].

For a finite-size particle ($0.05 \leq \frac{a}{D_h} \leq 0.2$), Di Carlo et al. [8] calculated the inertial lift forces taking into account the finite-size effects of the suspended particles. Near the channel centre, where the effects of the wall are weak, the lift force scales as:

$$F_L \propto \rho_f U_f^2 a^4 / D_h^2 \quad (2.17)$$

While near the channel wall, wall effects dominate, and it scales as:

$$F_L \propto \rho_f U_f^2 a^6 / D_h^4 \quad (2.18)$$

2.7 Dean Flow Drag Force

Considering a channel with a curvature, a gradient of pressure between internal and external wall appears.

The gradient is equal in all the cross sections of the channel. In the external part of the cross section, there is a big pressure with respect to the inner part of the curvature because the velocity is greater on the outside of the channel and here a secondary force called Dean force appears.

The centrifugal force pushes the fluid toward the external part of the curvature. Since the walls are also up and down the cross section of the channel, at the central part of cross section there is a linear momentum bigger with respect to the walls up and down the cross section, because the velocity is zero there. Since that at the centre of the cross section there is larger velocity, a bigger centrifugal force is felt and so wants to go toward the external part. When going toward the external part of the curvature, the fluid is found to stay close to the wall. The centrifugal force is big and is able to move the flow close to the wall and this flow will move from the top or bottom of the cross section creating some vortexes that push the slow fluid toward the internal part of the cross section. These up and down vortexes are created and are called Dean vortexes (Figure 2.4 can be seen).

If the density of the particle is very close to that of the fluid, the effect of the particle centrifugal force around channel curvatures is negligible and so there is only inertial lift force and Dean drag force.

A parameter that influences the strength of the secondary flow is the Dean number [9] defined in this way:

$$De = Re \sqrt{\frac{D_h}{2R_c}} = \frac{\rho v D_h}{\mu} \sqrt{\frac{D_h}{2R_c}} \quad (2.19)$$

R_c is the radius of curvature of the channel(internal radius).

D_h is the hydraulic diameter of the channel.

The velocity of this lateral migration of particles is called the Dean velocity (U_{Dean}) and can be calculated by the following expression [10]:

$$U_{Dean} = 1.8 \times 10^{-4} De^{1.63} \quad (2.20)$$

And the Dean drag force, estimated by Stokes' law, is:

$$F_{Dean} = 3\pi\mu U_{Dean} a = 5.4 \times 10^{-4} \pi a \mu De^{1.63} \quad (2.21)$$

Inertial focusing often utilizes Dean flow drag force, because often times the difference in equilibrium positions created by the balance of the wall lift force and the shear gradient lift force of different sized particles is not substantial enough to effectively separate them.

Small sized particles were transposed by the Dean drag force towards the outer wall of the channel. Larger particles, however, found lateral equilibrium positions closer to the inner wall of the channel as a consequence of the Dean drag force coupled with inertial lift force. Therefore, particles of different sizes will be focused in distinct streams and could be collected from different outlet channels. Particles

with $\left(\frac{a}{D_h}\right) > 0.07$ are balanced at the inner wall instead if $\left(\frac{a}{D_h}\right) < 0.07$ are entering in the Dean vortices.

It was seen that a loss of focusing occurred at $\left(\frac{a}{D_h}\right) < 0.07$ and $De > 20$ [11].

Earlier work by Chun and Ladd [12], showed preferential focusing for particles with $\left(\frac{a}{D_h}\right) > 0.12$ and was later confirmed by Di Carlo and Bhagat, this is due to the micro particles being too small to be significantly impacted by the inertial lift forces. Focusing behavior is also impacted by the volume fraction of the particles in the suspension. The volume fraction is generally restricted to $< 1\%$, otherwise, particle-particle interactions disrupt the focusing.

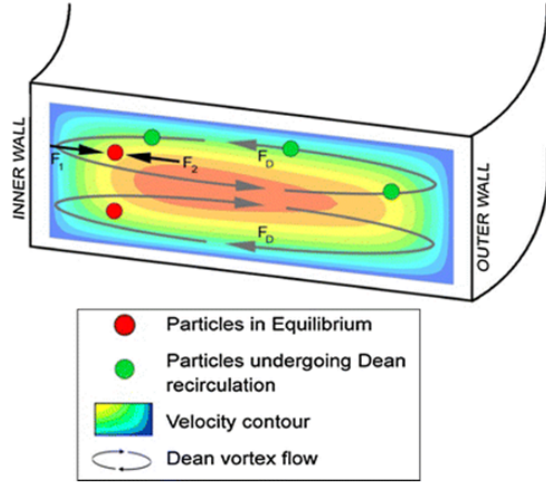


Figure 2.4: in this figure it is shown that due to curvature of channel, the fluid goes to the outer wall which results in the creation of the Dean vortex. The small particles (green particles) are entering in the Dean vortex and are not in equilibrium instead the bigger particles (red particles) found an equilibrium position close to the inner wall

If $De > De_c$ an additional vortex exists, Figure 2.5. The secondary vortices trap the particles towards the concave wall, not allowing focusing.

The presence of a secondary vortex for $De > De_c$ has an important effect of particles focusing.

Their job is to shift the particles stream focusing from the convex to the concave wall.

An aspect ratio for rectangular or square section can be defined:

$$AR = \frac{H}{W} \quad (2.22)$$

Furthermore, it has been shown that De_c is inversely proportional to $AR^{0.5}$ ($De_c \propto AR^{-0.5}$), so as AR increases, De_c decreases, as shown in Figure 2.6. For this reason, rectangular section channels with low AR are used, Figure 2.7.

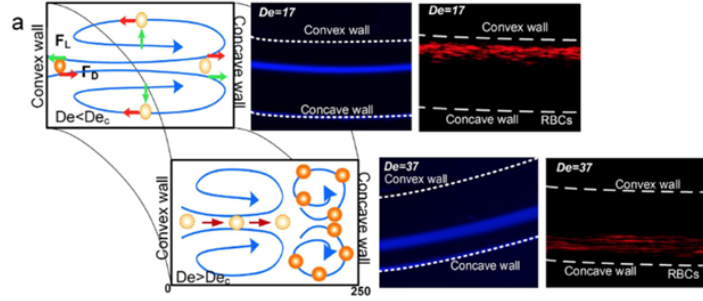


Figure 2.5: secondary vortex

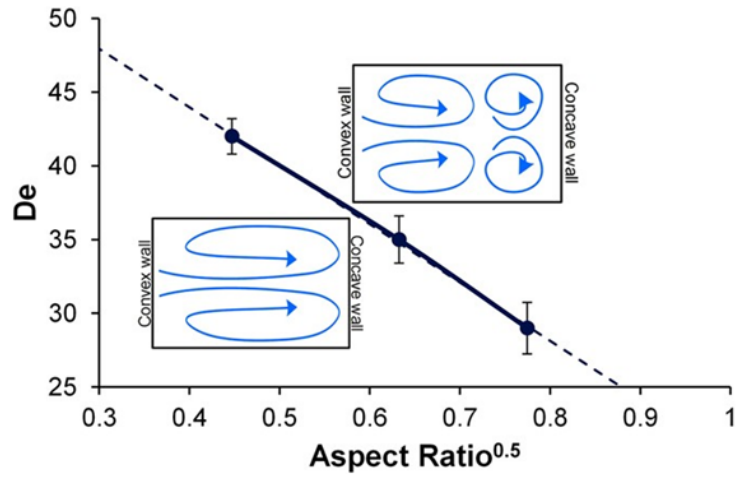


Figure 2.6: in this figure it has shown the relation between De_c and $AR^{0.5}$

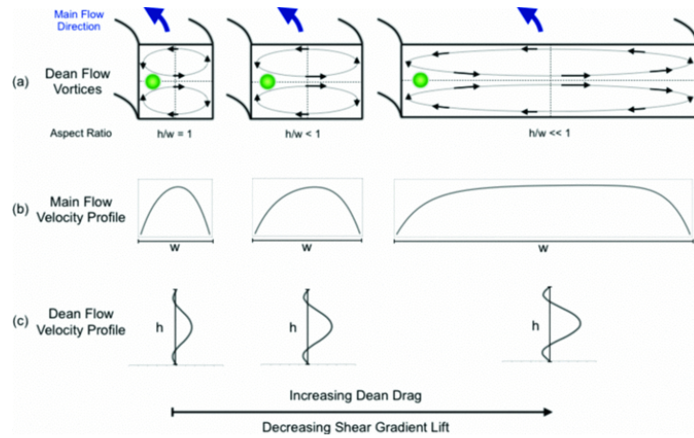


Figure 2.7: this figure illustrates how the aspect ratio influence the Dean flow

The ratio of net inertial lift force to the Dean drag force is:

$$R_f = \frac{a^3 R_c}{D_h^3} \quad (2.23)$$

and it determines the relative position where particles of various sizes will gather within the channel. Dean drag force is dominant when R_f approaches 0, and this condition is true for particles with size much smaller than the channel hydraulic diameter. In this case, Dean force drives small particles closer to the channel outer wall that is closer to the platform edge. On the other hand, as R_f approaches infinity, inertial force is dominant for large particles with diameter similar to channel hydraulic diameter. Therefore, large particles are flowing close to the inner wall of the curved channel which is closer to the platform centre.

A too small value of R_f would generate chaotic particle motion instead of deterministic particle focusing.

To have particles focus and successfully separate in the microfluidic channels, several conditions have to be met.

Sprenger et al., discovered that the Dean number must be greater than 1 and lower than 11.[19], the ratio of particle diameter and hydraulic diameter must be $\left(\frac{a}{D_h}\right) > 0.12$.

Dutz et al.[20] found that the minimal length of the channel must be:

$$L_{min} = \left(\frac{3\pi\mu_f}{2\rho v_f} \right) (L_c/a)^2 \quad (2.24)$$

Where L_c is the characteristic length that is the shortest dimension of the rectangular cross section and v_f is the velocity of the fluid.

Increasing the flow rate, the Dean number is increased and thus it can be done until a single focused particle stream is formed at the outlet.

Increasing the flow rate further, implies a migration of the focused particle stream away from the inner wall channel towards the channel of the center due to the fact that the Dean force becomes important.

If the flow rate is increased further, the Dean force becomes dominant with respect to the net lift force and so there is a de-focusing of particles.

In Figure 2.8 it is shown that by increasing the flow rate, the Dean number is increased and the streamline is shifted to the center. The shift and so the increasing of the Dean number can be also done increasing the hydraulic diameter (e.g. constant W and changing the H).

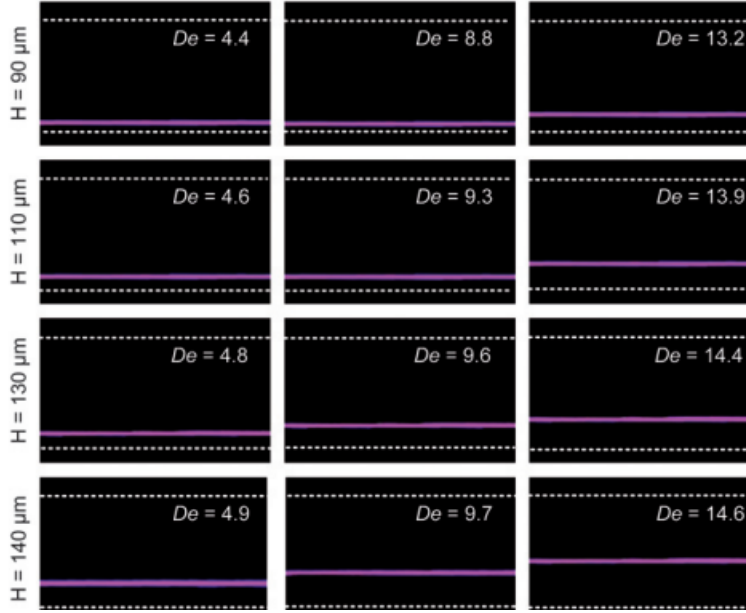


Figure 2.8: results using a spiral channel with $W = 500\mu m$ and particles of $10\mu m$

2.8 Cross Section

There are several different cross section shapes used in the field of inertial focusing. However, the three most common shapes are a square, rectangular and circle. In a square channel, randomly sorted particles will migrate to four equilibrium positions near the center of each wall face based on the balance of the wall lift force and shear gradient force.

In the case of rectangular cross section, since that there is a small and a big edge, the particle reaches equilibrium in 2 positions, in a low aspect ratio ($AR \approx 0.5$) channel, particles focus at the centre about $0.2H$ away from the long walls.

In the case of circular channels, an annulus of equilibrium positions occurs at 0.6 times of the channel radius from the axis [15], as can be seen in Figure 2.9.

A recent area of study using trapezoidal cross sectional areas, has shown an increase in separation of differently sized particles compared to previous channels. This is seemingly due to an increase in the Dean flow velocity gradient for trapezoids. The most significant difference between differently shaped cross sections is that inertial forces will be stronger for smaller dimension cross sections, resulting in focusing occurring sooner.

In a squared cross section channel, if the velocity is increased, the particles are slowly shifted toward the wall having the same equilibrium shape. In rectangular cross sections, by increasing the velocity, it is possible to pass from two positions to four position of equilibrium, as it is shown in Figure 2.10.

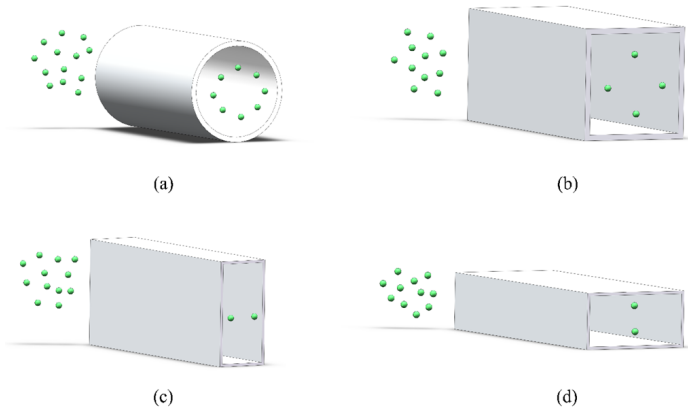


Figure 2.9: How the shape of the cross section influences the focusing position

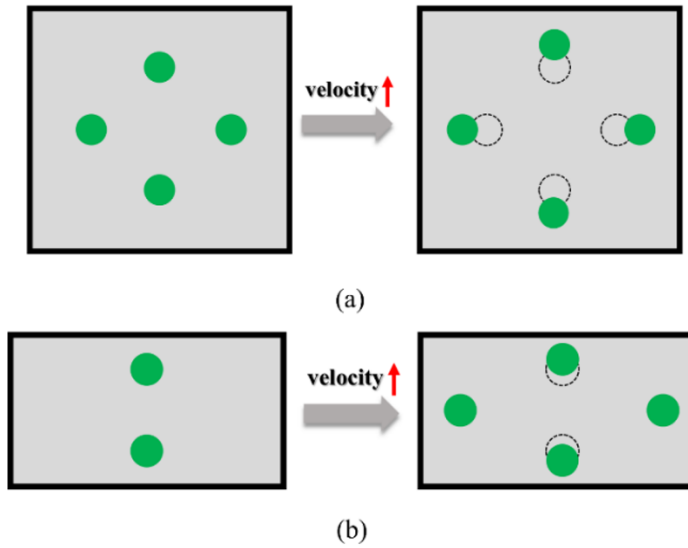


Figure 2.10: increment of velocity and changing of equilibrium position

There is the possibility to have a single stream line focusing using a straight channel with a triangular cross section with a tip angle of 120° .

It has been studied that the single focusing occurs at less than 3cm at a flow rate of $100\mu\text{l}/\text{min}$, Figure 2.11.

Recently, it was shown that it is possible to focus particles at a single position using these low aspect ratio channels with triangular cross-sections, at relatively low flow rates ($Re = 29 - 44$) [16]. It is known that in a low AR rectangular micro channel, the point of maximum velocity is at half of the channel height ($0.5H$). In contrast, the point of maximum velocity for low AR triangular cross section, shifts to $0.4H$ as can be seen in Figure 2.11.

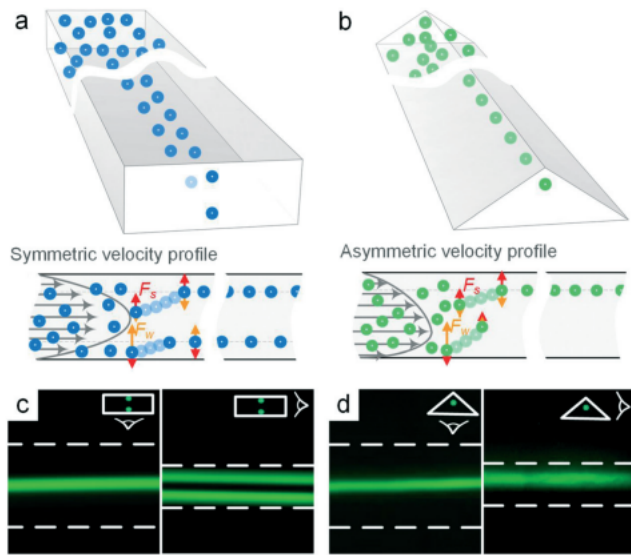


Figure 2.11: rectangular with $W = 100\mu\text{m}$, $H = 40\mu\text{m}$ and triangular 120° cross section

The results [16] shows that at lower flow rates ($Re < 29$), the $15\mu\text{m}$ diameter particles did not achieve 3D focusing throughout the 5 cm downstream length of the micro channel, as the inertial lift forces were not sufficiently high. At $Re = 29$, the $15\mu\text{m}$ diameter particles randomly distributed at the inlet begin to migrate toward the top of the channel in 1 cm of length but a better focusing occurs when 5cm of length is reached.

At high Reynolds number $Re = 190$ there is not one single stream line focusing but 3, as can be seen in Figure 2.12.

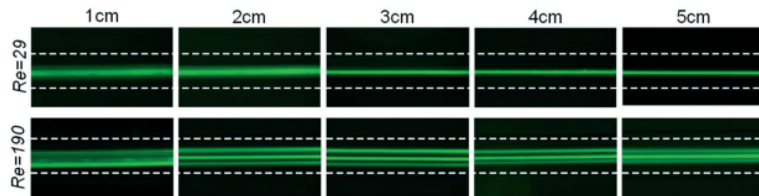


Figure 2.12: particle focusing of $15\mu\text{m}$ at different flow rates

2.9 Comparison between trapezoidal and rectangular cross sections

The trapezoidal cross section, generates a large Dean vortex near the outer wall of the the channel and so this implies that small particles are trapped in the vortex, instead larger particles which remain at the inner wall. In this way, a better separation between different particles can occur.

The generic formula for the hydraulic diameter is:

$$D_h = 4 \cdot \frac{\text{area}}{\text{perimeter}} \quad (2.25)$$

in the case of trapezoidal cross section the formula becomes:

$$D_h = \frac{2(H+h)W}{H+h+W+\sqrt{H^2-2Hh+h^2+W^2}} \quad (2.26)$$

In the rectangular cross section, the focusing position of particles of the same type moves from the inner to outer wall gradually increasing the flow rate.

It has been studied that the equilibrium position of the particles along the height of the channel, does not depend on the flow rate but remains constant at $22.0 \pm 1.1\%$ of channel depth from top and bottom wall for a range of flow rate of $0.5 - 7.5 \text{ mL/min}$ [14], as can be seen in Figure 2.13:

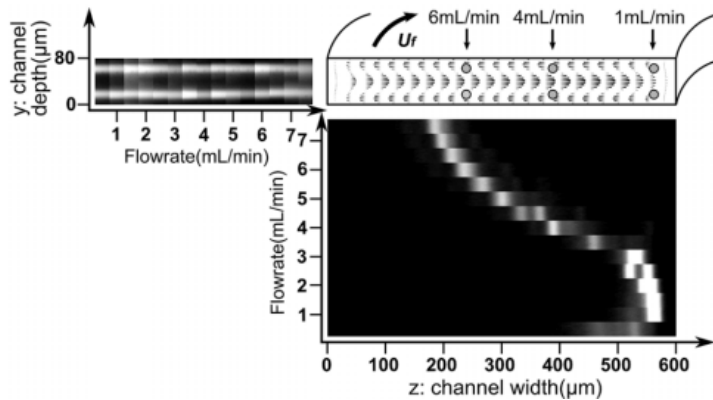


Figure 2.13: Focusing position in a rectangular cross section

For the trapezoidal cross section, the behaviour is similar at low flow rates but after a certain threshold of flow rate the particles suddenly go to the outer wall of the channel. The threshold flow rate is a function of particle size and increases with them.

The particles are trapped in the center of the two Dean vortex.

Looking at the height of the cross section, the particles are focused at $25.5 - 27.1\%$ of the channel depth, as it is shown in Figure 2.14:

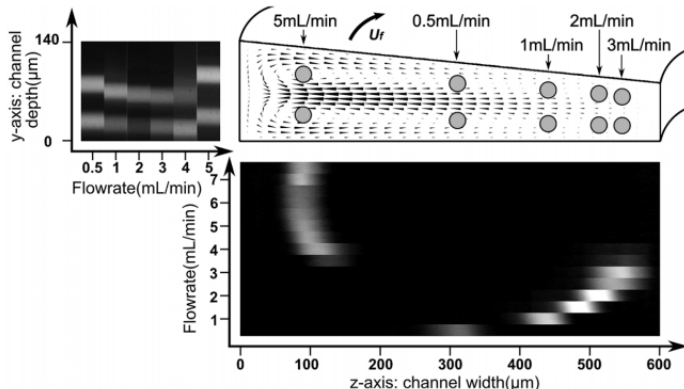


Figure 2.14: Focusing position in a trapezoidal cross section

Considering a large slope angle, there will be a strong Dean at the outer side wall and increased trapping capability of particle. Large slope angles can also decrease the threshold flow rate required to trap the particles of certain size within the Dean vortices.

2.10 The effect of inward and outward slopping of trapezoid cross section

It has been studied that with equal hydraulic diameter, the particles initially dispersed in the channel migrate into a well ordered streamline located very tight to the inner wall in the case of inward sloping(the bigger height of the trapezoid is in the inner wall) unlike the outward sloping.

In the outward sloping (the bigger height of the trapezoid is in the outer wall) the particles are focused in the middle of the channel and is not tight, Figure 2.15.

It has also been documented that the size of particles influence the degree of focusing due to the fact that the net lift force is proportional to a^4 and the Dean force to a . The larger the particles and the greater focusing that can be achieved.

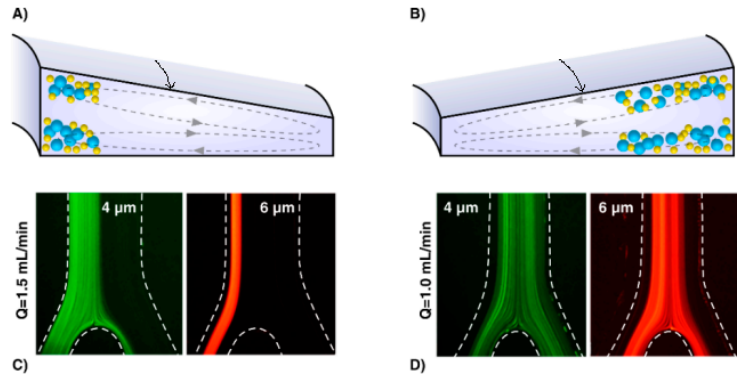


Figure 2.15: how the position of the outer wall respect to the flow direction can influence the focusing of particles

2.11 Straight Channel Length

The following length equation has been theorized by Di Carlo using the balance of the net lift force (eq.2.15) and Stokes drag force (eq.2.5). This equation intends to aid in the design of an inertially focused device but is not precise due to the complexity of the force balance:

$$U_L = \frac{F_L}{3\pi\mu a} = \frac{\rho_f U_f^2 a^3}{6\pi\mu D_h^2} \quad (2.27)$$

$$L_{min} \approx \frac{D_h}{2U_L} U_f = \frac{3\pi\mu_f D_h^3}{\rho_f U_f a^3} \quad (2.28)$$

It should be noted that for a correct interpretation, the inertial particle focusing should be considered as a balance of the net pressure and viscous forces, and not simply by calculating the Re (channel Reynolds number), which does not include particle information. Therefore, it is worthwhile to introduce another dimensionless parameter for predicting the particle focusing, called the particle Reynolds number, Re_p , which is defined as follows:

$$Re_p = Re \left(\frac{a}{D_h} \right)^2 \quad (2.29)$$

Low focusing efficiency is shown when $Re_p \ll 1$, because particles are subjected to the dominant viscous drag to follow fluid streamlines. Focusing occurs only if $Re_p \sim 1$ because inertial lift forces become dominant and lateral migration of particles across the fluid streamlines becomes evident. Exceeding the critical value of Re , the number of stable positions vary according to a function dependent on the size of the particle, the size of the channel and on Re . Liu has defined a critical value of the Reynolds number below which the number of equilibrium positions assumed by the suspended particles is minimal:

$$Re_c = 697 \left(\frac{AR}{k} \right)^{-0.79} \quad (2.30)$$

Where k is the ratio between the diameter of the particle (approximate to a sphere) and the smaller side of the channel section (typically the height H), $4.5 \leq AR, k \leq 60, 5 \leq Re \leq 660$.

When $Re \gg Re_c$, the particle migration behaviour is no longer predictable.

2.12 Serpentine Micro channel

The curvature direction of the serpentine micro channel is not constant, which makes the Dean flow's effects on particle migration much more complicated. There are two kind of spiral micro channels, symmetric and asymmetric.

In the symmetric serpentine micro channel, particles are focused at two side equilibrium positions, and this focusing condition would be disturbed by increasing flow rate. In the asymmetric serpentine micro channel, particles are concentrated to the single streamline in the center of channel, and this equilibrium position can change increasing the flow rate. Using the asymmetric channel there is also highly regulated inter-particle spacing.

When high velocity inlet is used, the low elastic modulus of the material of the channel, that is polydimethylsiloxane (PDMS), makes its use problematic for this microfluidics application because there is a cross-section deformation and a loss of focusing.

The benefit of using high flow rates is that a lower length of the channel is needed to have the focusing. The net lift force is the dominant focusing mechanism moving particles to their equilibrium positions; the Dean force does not focus particles, but it reduces the number of equilibrium positions from four to one and to speed up the focusing process.

Small size particles requires a higher flow rate with respect to larger particles in order to obtain a

sufficiently large lift force (eq. 2.15 can be seen).

When $R_f > 0.4$ (eq.2.23) a stable equilibrium occurs.

It was discovered that the particles are focused if the thickness of the straight particle line (FWHM) is less than twice particle diameter.

It has been seen that the channel length can vary from 3 to 9 mm having almost the same result of focusing when high flow rate like $700 \mu\text{L}/\text{min}$ is used, instead if low flow rates is used, there is a range from 2 to 3 cm of total length.

It was seen that by increasing the flow rate the degree of focusing increase (Figure 2.16 can be seen).

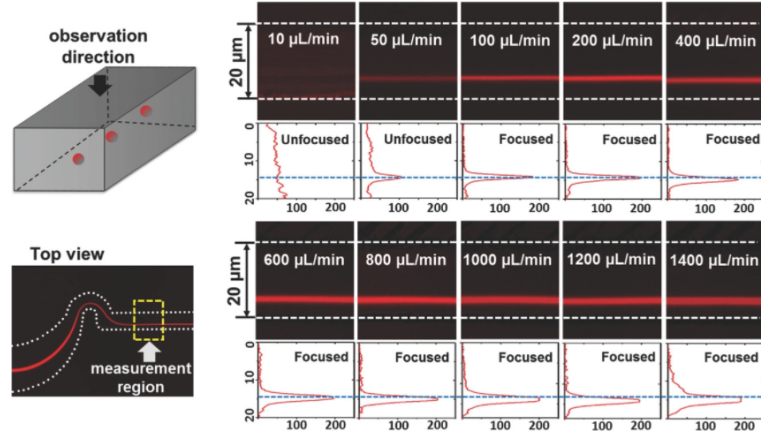


Figure 2.16: how the flow rate can change the focusing

Also changing the concentration of the particles can change the focusing due to the particle-particle interaction, Figure 2.17.

The length ratio λ , that is the ratio of number particles diameter per channel length, was introduced and can be expressed in this way:

$$\lambda = \frac{aA_c V_f}{V_p} = \frac{6WHV_f}{\pi a^2} \quad (2.31)$$

where V_f is the suspension volume fraction and A_c is the channel cross-sectional area.

When $\lambda < 0.5$ there can be a single train of aligned particles; when $\lambda > 0.5$ there are two lines and when $\lambda > 1$ three.

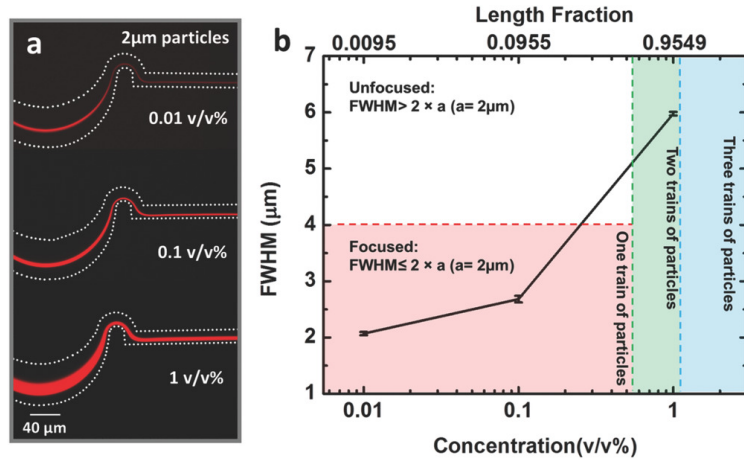


Figure 2.17: how the concentration of particles influence the focusing

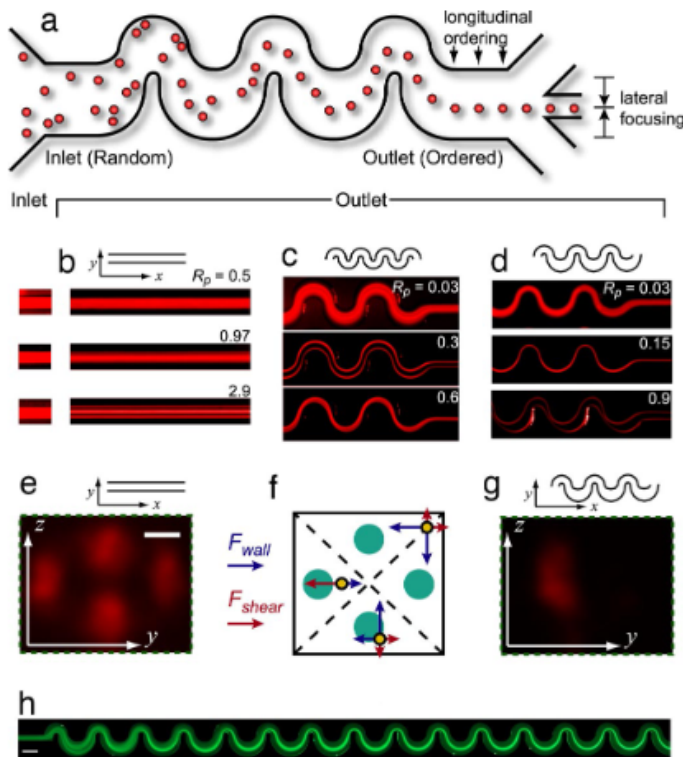


Figure 2.18: shape and length of spiral micro channel

2.13 Distance between particles

It was observed that changing the section area of the channel doing a symmetric expansion and contraction, there is an increased distancing between particles and inter particle spacing downstream

does not return to its original value, as is laid out in Figure 2.19.

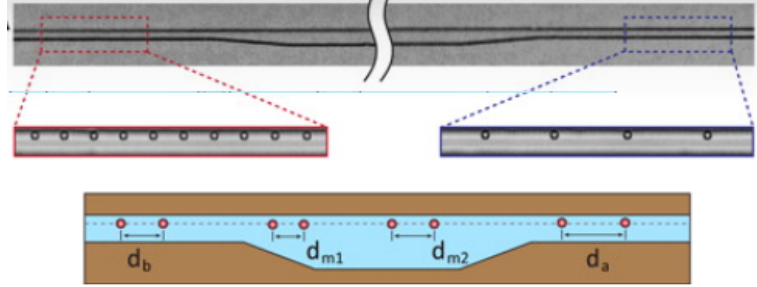


Figure 2.19: increment of spacing between particles

When the particles enter in the expansion of the channel with a certain distance d_b , for the conservation of the mass the velocity must decrease and the particles in a first moment are closer $d_{m1} < d_b$. Due to the particles being close to each other, there is a viscous repulsive interaction causes the separation of them and so increasing the distance to $d_{m2} > d_{m1}$. Finally, when the channels change their dimensions again, there is an increasing of the velocity as well as the increased separation of the particles with respect to the initial value $d_a > d_b$.

This increasing of distance can occur only for particles that have a distance $d_b < 100\mu m$, in the other case $d_a = d_b$, (Figure 2.20 can be seen).

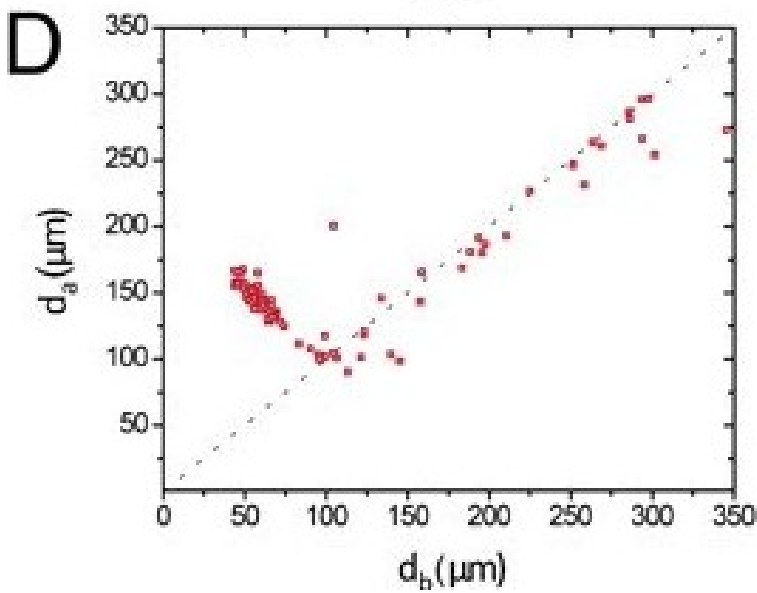


Figure 2.20: the increasing of particle space for a certain initial space d_b

The changing of the channel can be done in this way: length of the expansion region of 2mm and width increased of $20\mu m$.

Chapter 3

DPM IN ANSYS FLUENT

3.1 Introduction

The Lagrangian discrete phase model (DPM) in ANSYS FLUENT, follows the Euler-Lagrange approach.

The fluid phase is treated as a continuum by solving the Navier-Stokes equations, while the dispersed phase is solved by tracking a large number of particles, bubbles, or droplets through the calculated flow field. The dispersed phase can exchange momentum, mass, and energy with the fluid phase.

A fundamental assumption made in this model is that the dispersed second phase occupies a low volume fraction, although high mass loading ($\dot{m}_{\text{particles}} \geq \dot{m}_{\text{fluid}}$) is acceptable. The particle or droplet trajectories are computed individually at specified intervals during the fluid phase calculation. This makes the model appropriate for the modeling of spray dryers, coal and liquid fuel combustion, and some particle-laden flows, but inappropriate for the modeling of liquid-liquid mixtures, fluidized beds, or any application where the volume fraction of the second phase cannot be neglected.

3.2 Particle Motion Theory

In Figure 3.1 it is shown some very light particles in the fluid flow (negligible mass).

They are injected into the flow and, as can be seen, the light particles tend to follow the stream lines of the flow.

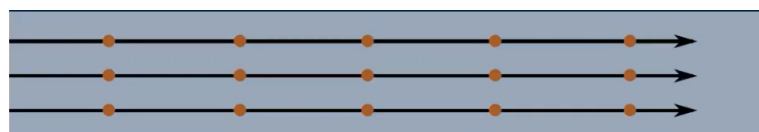


Figure 3.1: small particles follow the stream lines

In Figure 3.2 instead, it is shown that heavy particles must fall down towards the bottom of the pipe and it is expected that them have to follow a curved trajectory and move downwards.

In this case, an incorrect answer will be given which means a different approach will be needed in order to account for the particle mass.

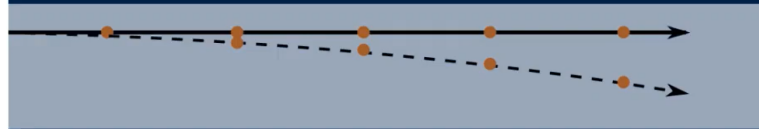


Figure 3.2: heavy particles do not follow the stream lines

In addition to the particles moving down towards the bottom of the pipe, it is also expected the particles will move slower than the fluid and the reason for this is due to drag (can be seen in Figure 3.3).

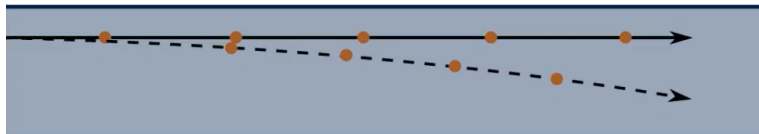


Figure 3.3: heavy particles do not follow the stream lines and are subjected to drag

For heavy and larger particles, streamlines cannot be used to track the trajectory of these particles but a different technique called Lagrangian particle tracking must be used.

If a streamline to track particle trajectory is used, the following differential equation must be solved to update the particle position \mathbf{x}_p :

$$\frac{d\mathbf{x}_p}{dt} = \mathbf{U}_p \quad (3.1)$$

Where \mathbf{U}_p is the particle velocity vector.

If the particles have no mass, it has been seen that the particle velocity is equal to the local fluid velocity in the cell of the CFD mesh ($\mathbf{U}_p = \mathbf{U}$), that means that eq.(3.1) can be solved if it is known what the fluid velocity is.

To solve the eq.(3.1) is used an Euler explicit time stepping approach:

$$\frac{\mathbf{x}_p^{i+1} - \mathbf{x}_p^i}{\Delta t} = \mathbf{U}_p^i \quad (3.2)$$

$$\mathbf{x}_p^{i+1} = \mathbf{x}_p^i + \mathbf{U}_p^i \cdot \Delta t \quad (3.3)$$

Where \mathbf{x}_p^i is the current particle position, \mathbf{x}_p^{i+1} is the next particle position that it wants to find and Δt is the time step.

The particle is moved from one location in the CFD mesh to another point in the CFD mesh.

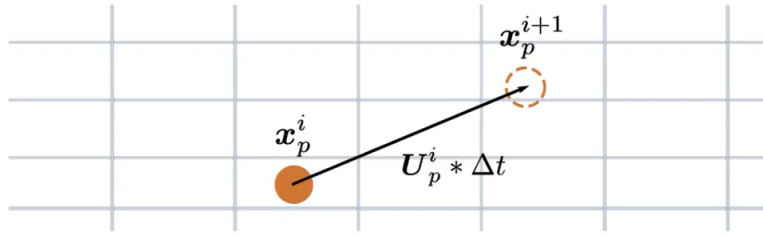


Figure 3.4: particle moving in the mesh

Basically the eq.(3.3) is used over and over, continuing to update the particle position until a complete particle trajectory is achieved and it is possible to workout the entire motion of a single particle through the fluid flow field.

For a particle with mass, the velocity of the particle is different from the local fluid velocity in the mesh and the trajectory is different from the fluid streamline. In this case a force balance on the particle must be used to workout what the particle velocity is.

Newton's second law for solid particle with mass must be used:

$$\mathbf{F} = m_p \mathbf{a} = m_p \frac{d\mathbf{U}_p}{dt} \quad (3.4)$$

$$m_p \frac{d\mathbf{U}_p}{dt} = \mathbf{F}_{drag} + \mathbf{F}_{buoyancy} + \mathbf{F}_{others} \quad (3.5)$$

in Figure 3.5, it is shown a spherical particle moving in a stationary fluid.

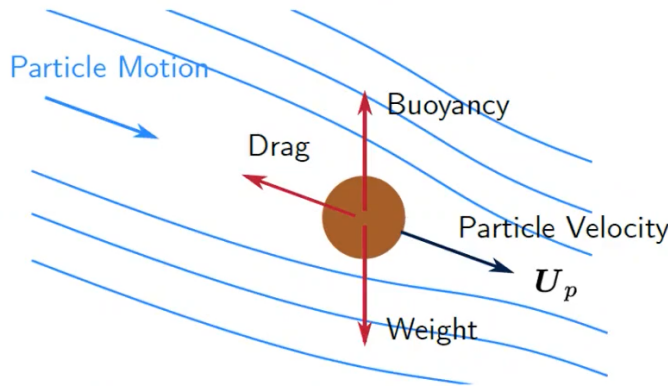


Figure 3.5: motion of a particle in a fluid

The weight of the particle acts in the direction of \mathbf{g} :

$$F_{weight} = \rho_p \mathbf{g} V_p \quad (3.6)$$

The buoyancy acts in the direction of $-\mathbf{g}$:

$$F_{buoyancy} = -\rho_f \mathbf{g} V_p \quad (3.7)$$

The net force is in the direction of \mathbf{g} :

$$F_{vertical} = (\rho_p - \rho_f) \mathbf{g} V_p \quad (3.8)$$

The general form of the drag force is:

$$F_{drag} = \frac{1}{2} \rho f_{drag} U^2 A \quad (3.9)$$

Where A is the projected area in the direction of the flow.

For a particle moving in a fluid, drag acts in the direction $\mathbf{U} - \mathbf{U}_p$ and the eq.(3.9) can be written in this way:

$$\mathbf{F}_{drag} = \frac{1}{2} \rho f_{drag} |\mathbf{U} - \mathbf{U}_p| (\mathbf{U} - \mathbf{U}_p) A_p \quad (3.10)$$

The projection of the sphere particle is the area of the circle.

Drag on a sphere is a function of the particle Reynolds number Re' , the plotting of the function can be seen in Figure 3.6 :

$$\begin{cases} \frac{24}{Re'} (1 + 0.15 Re'^{0.687}) & Re' < 1000 \\ 0.44 & Re' > 1000 \end{cases} \quad (3.11)$$

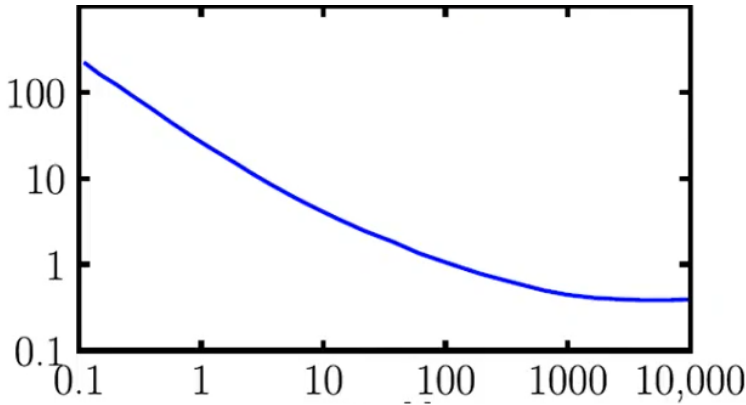


Figure 3.6: plot of the drag function depending on Re'

where the particle Reynolds number is:

$$Re' = \frac{\rho d_p |\mathbf{U} - \mathbf{U}_p|}{\mu} \quad (3.12)$$

The eq.(3.11) is the Schiller-Neumann model.

Since the particle velocity is not known, the particle Reynolds number cannot be calculated and therefor drag coefficient as well.

The particle velocity can be used from the previous time step of the Lagrangian track to calculate the particle Reynolds number in order to identify the drag coefficient.

Once calculated, the following balance equation is solved to calculate the particle velocity:

$$m_p \frac{d\mathbf{U}_p}{dt} = \frac{1}{2} \rho f_{drag} |\mathbf{U} - \mathbf{U}_p| (\mathbf{U} - \mathbf{U}_p) A_p + (\rho_p - \rho_f) \mathbf{g} V_p \quad (3.13)$$

finally the particle position is updated using the following equation:

$$\mathbf{x}_p^{i+1} = \mathbf{x}_p^i + \mathbf{U}_p^{i+1} \cdot \Delta t \quad (3.14)$$

This sequence of calculations is done for each time step and for each particle.

ANSYS FLUENT simplifies the eq.(3.13) by completing it as follows:

the eq.(3.13) is divided by the mass of the particle ($m_p = \rho_p V_p$) and then the first term top and bottom multiplied by d_p and μ :

$$\frac{d\mathbf{U}_p}{dt} = \frac{1}{\rho_p V_p} \left(\frac{f_{drag} \mu}{2 d_p} \right) Re' (\mathbf{U} - \mathbf{U}_p) A_p + \left(\frac{\rho_p - \rho_f}{\rho_p} \right) \mathbf{g} \quad (3.15)$$

Substituting V_p and A_p , the following equation is obtained:

$$\frac{d\mathbf{U}_p}{dt} = \left(\frac{18\mu}{\rho_p d_p^2} \right) \left(\frac{f_{drag} Re'}{24} \right) (\mathbf{U} - \mathbf{U}_p) + \left(\frac{\rho_p - \rho_f}{\rho_p} \right) \mathbf{g} \quad (3.16)$$

in a compact form:

$$\frac{d\mathbf{U}_p}{dt} = F_D (\mathbf{U} - \mathbf{U}_p) + \left(\frac{\rho_p - \rho_f}{\rho_p} \right) \mathbf{g} \quad (3.17)$$

The particle relaxation time can be defined as:

$$t_p = \frac{\rho_p d_p^2}{18\mu} \quad (3.18)$$

The particle relaxation time is a measure of how quickly it takes a particle to respond to changes in the flow field.

If a particle is moving along a streamline and if it has a very small particle relaxation time, then when the flow field changes (the streamline curves for example) or if there is any unsteadiness in the flow field, the particle will quickly adjust to the course of the flow field and be able to follow the streamlined very closely.

On the other hand for example if there is a large particle relaxation time, a particle will take a long time to respond to changes in the flow field and that means that particle will not tend to follow the streamlines and will tend to fall out of the fluid very quickly. An example can be seen in Figure 3.7.

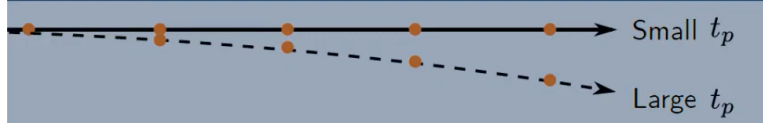


Figure 3.7: small t_p the particle follow the stream line, large t_p the particle is not able to follow the stream line

In the Stokes regime it is known that the particles Reynolds number tends to 0 and from the eq.(3.11) the drag coefficient is:

$$f_{drag} = \frac{24}{Re'} \quad (3.19)$$

Putting this in the eq.(3.17) and solving the differential equation with an initial condition that the particles at time $t=0$ is rest, the following result is obtained:

$$U_p(t) = U \left(1 - \exp \left(-\frac{t}{t_p} \right) \right) \quad (3.20)$$

A dimensionless number called particles Stokes number can be defined:

$$St_p = \frac{t_p}{t_f} = \frac{\text{particle relaxation time}}{\text{fluid time scale}} \quad (3.21)$$

The Stokes number can be seen also in another way:

$$St_p = \frac{t_p \cdot U}{l_f} \quad (3.22)$$

Where $t_p \cdot U$ is the distance in which the particle will reach the velocity of the fluid (steady state) and l_f is the length scale of the fluid that correspond with the hydraulic diameter of the channel.

If the particle has $St_p \ll 1$ this means that will follow the fluid streamline.

Chapter 4

ANSYS FLUENT SIMULATION

4.1 Test spiral micro channel to capture Dean vortexes

The aim of this section is to identify the number of cells required in the computational domain to obtain an accurate and converged solution of the flow fields.

In the spiral micro channel the Dean vortex appears and to capture them a high resolution of mesh in the cross section is needed.

The spiral configuration, can be seen in Figure 4.1:

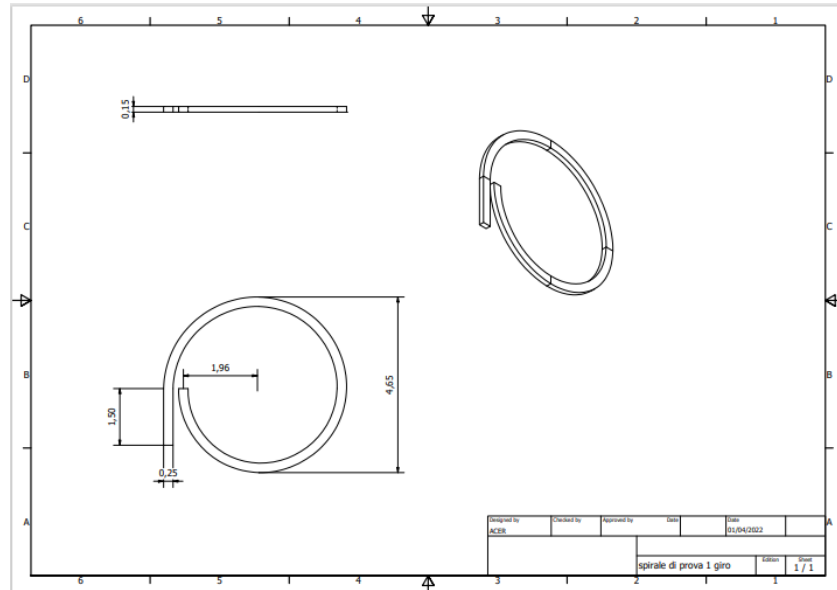


Figure 4.1: geometry of the spiral

The best trade off is to use a structured mesh with 2500 cells (51x51 nodes) in each cross section with an aspect ratio of cells equal to 2-2.5 in the curved channel and 3 in the straight channel, as it is shown in Figure 4.2.

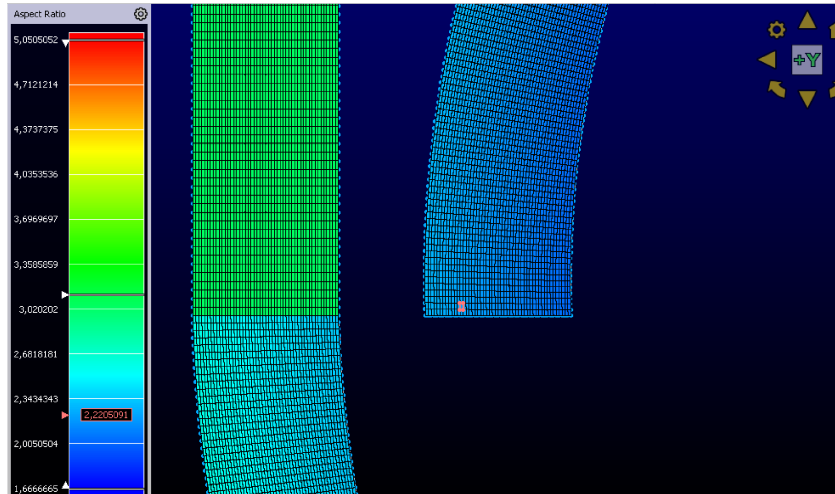


Figure 4.2: aspect ratio of the spiral

The aspect ratio of the channel cross section is 0.6.

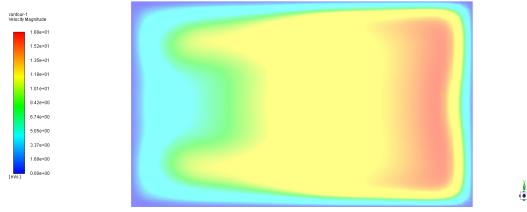


Figure 4.3: velocity contour $u=10\text{m/s}$

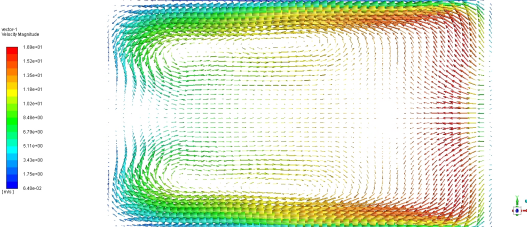


Figure 4.4: velocity vector $u=10\text{m/s}$

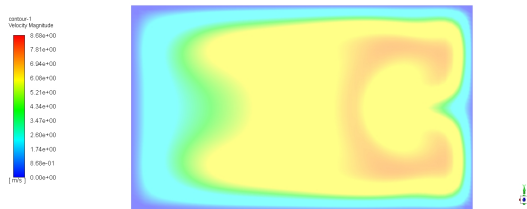


Figure 4.5: velocity contour $u=5\text{m/s}$

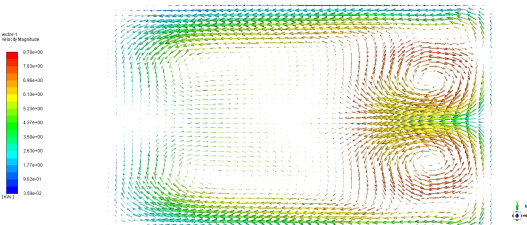


Figure 4.6: velocity vector $u=5\text{m/s}$

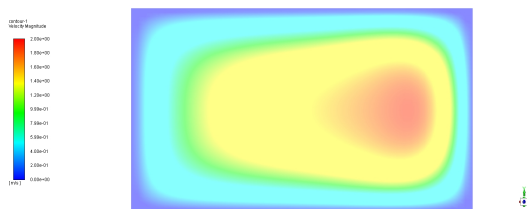


Figure 4.7: velocity contour $u=1\text{m/s}$

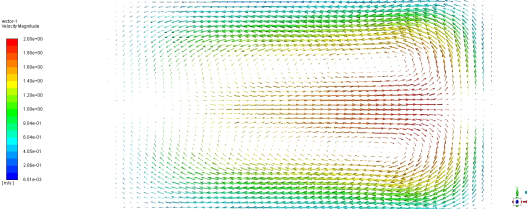


Figure 4.8: velocity vector $u=1\text{m/s}$

All these have been obtained reaching a residual lower than 10^{-4} .

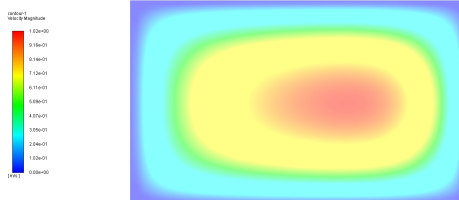


Figure 4.9: velocity contour $u=0.5\text{m/s}$

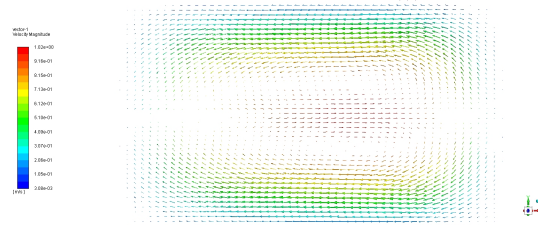


Figure 4.10: velocity vector $u=0.5\text{m/s}$

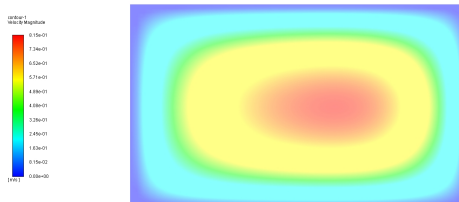


Figure 4.11: velocity contour $u=0.4\text{m/s}$

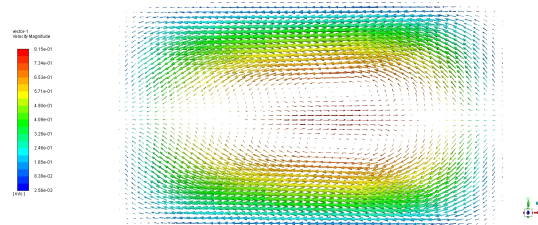


Figure 4.12: velocity vector $u=0.4\text{m/s}$

4.2 Experiment particle/parcels

In the discrete phase model, ANSYS replace particles with parcels. A parcel will appear as a "particle" and can be plotted in the domain, but it is actually a representative of a number (or even a fraction) of real particles. This depends on the total mass flow-rate and initial diameter/density values.

The aim of the simulation is to inject one particle every 0.001 second (that correspond to the step time) for a maximum number of particles of 5. These particles have a density equal to the water fluid.

The domain is a rectilinear channel where the inlet is the larger section and the outlet is the smaller section, as can be seen in Figure 4.13.

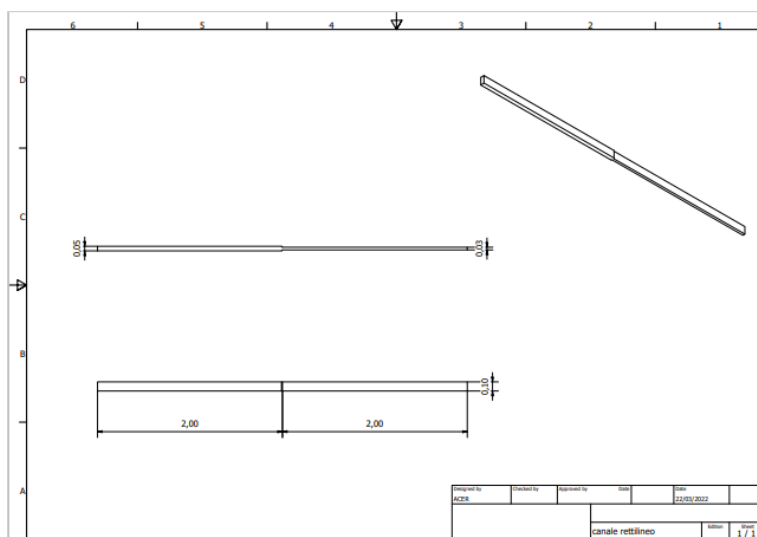


Figure 4.13: straight channel geometry

Basically, these particles act as fluid particles and therefore when the cross section area of the channel decreases, velocity increases to ensure mass conservation; the distance between particles increases as well.

The "single" type injection is used as injection.

The coordinate system is placed at the center of the inlet surface and in this case since the drawing of the channel was done in the XY plane, a x-velocity coordinate is used. When the center of inlet surface is used, a small x offset (e.g. 0.001mm) is needed, because there may be problems with the inlet of the particle, this is due to the fact that staying at $x=0$, the particles are on the boundary and cannot enter the domain.

The diameter of the particle is $20\mu m$ with a density of $998.2 kg/m^3$. The mass of the single particle is $4.181250382 \cdot 10^{-12} kg$.

It is possible to calculate the mass flow rate using the following equation:

$$\text{mass flow rate} = \frac{\text{particle mass} \cdot \text{number of particles}}{\text{time step}} \quad (4.1)$$

where the number of particles equals to 1, a mass flow rate of $4.181250382 \cdot 10^{-9} kg/timestep$ is obtained.

Before injecting the particles in the domain, a period of time must pass in order to have a low residual (e.g. 10^{-3}) at which point they be injected; if this is not done, a different solution may be obtained. A start time of 0.010 seconds and a stop time of 0.0141 seconds (it was used a delay of 0.0001 second due to computational errors) was used, in such a way to have a total of 5 particles.

The velocity inlet of the particle is $0.01 m/s$ and the velocity outlet is calculated using the conservation of the mass and is equal to $0.01667 m/s$.

The important thing when a transfer of particles is done, is to have not only a refined mesh along the cross section but also a refined mesh along the length of the channel because the complication of escape particles may arise.

In Figure 4.14 it is shown the mesh of the straight channel.

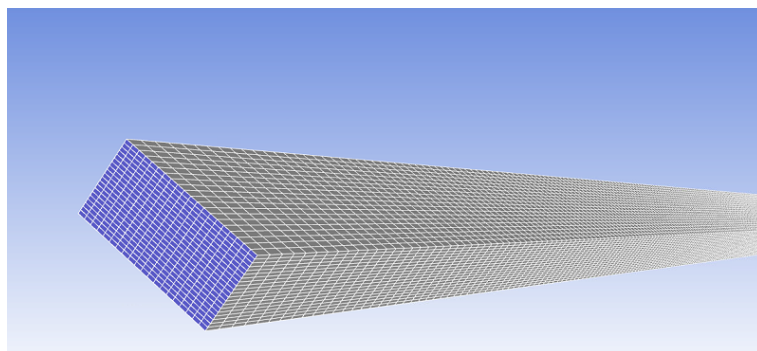


Figure 4.14: mesh geometry of straight channel

The result obtained during this simulation are correct with the real behaviour of the fluid particle. This can be seen in Figure 4.15.

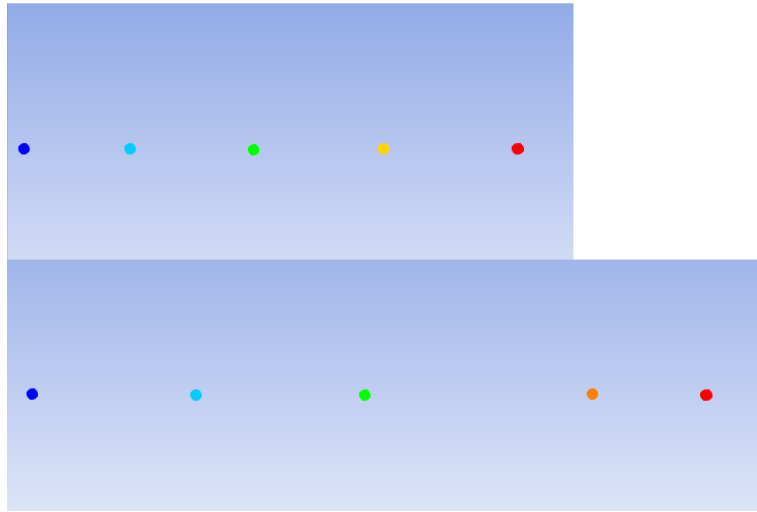


Figure 4.15: in the first picture the particles have a defined distance but when they reach the increasing of cross section, figure below, the distance is increased

4.3 Simulation of spiral micro channel

The goal of this project is to have an inertial focusing of particles using a spiral.

A sensor is put at the end of the spiral and it has to capture how many particles are going out.

The first step is to calculate the hydraulic diameter in such way $\left(\frac{a}{D_h}\right) > 0.07$. The smaller size of particle used in this experiment is $7\mu m$ and so a maximum hydraulic diameter of $0.1mm$ is obtained. The spiral chosen is composed by 5 loop, to guarantee enough length for focusing, and a straight channel placed at the end.

The particles have to enter from the center of the spiral and exit through the straight channel.

In this simulation as liquid was used water and the particles are described by a polystyrene material with a density of $1050kg/m^3$.

The total internal perimeter of the spiral is $133.273mm$.

It has been used $H = 0.05mm$, $W = 0.1mm$, as can be seen in Figure 4.16.

The hydraulic diameter is $0.06667mm$ and the aspect ratio is 0.5.

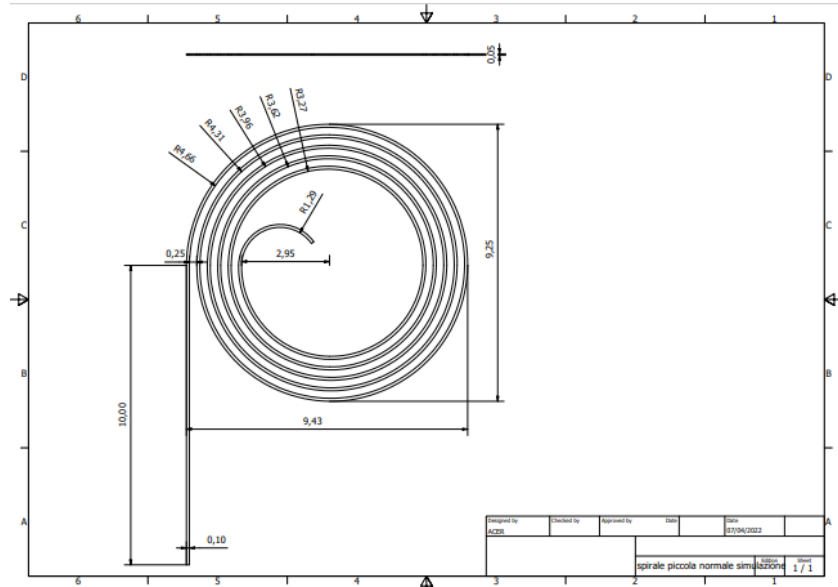


Figure 4.16: geometry of the spiral

It is possible to calculate how the Dean force increases with the increasing of the flow rate, using the eq.2.21, which yields the Dean force at the last loop of the spiral.

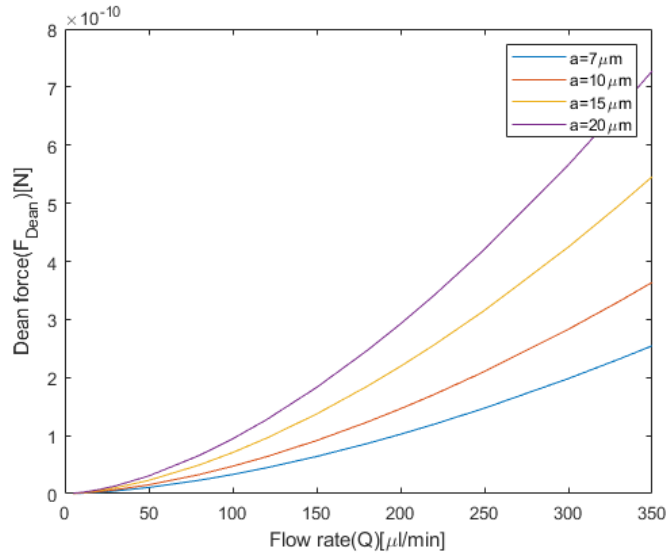


Figure 4.17: graph of the Dean Force over flow rate using MATLAB

If the range of flow rate that is used is magnified, it is easy to notice that there is not a significant difference when the particle size is increased:

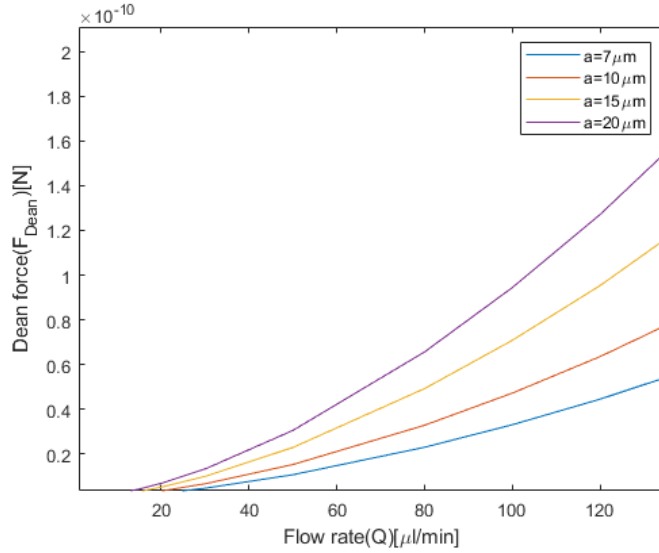


Figure 4.18: zoom of Figure 46

The Net lift force may be plotted using the eq.(2.15)(2.16):

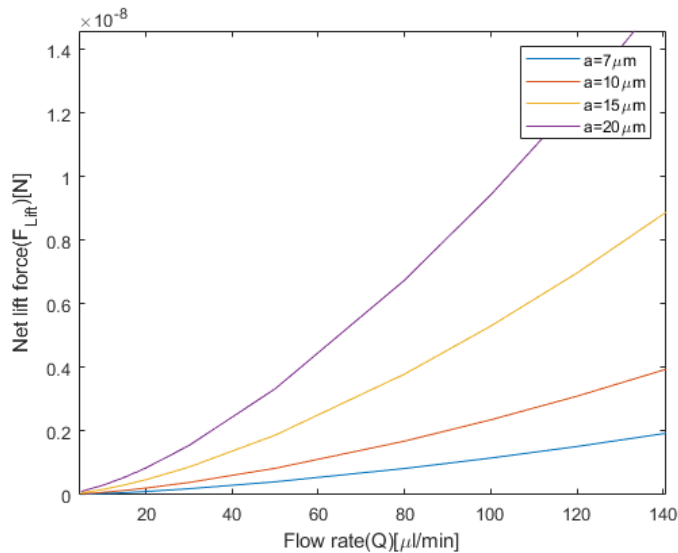


Figure 4.19: graph of the Net lift Force over flow rate using MATLAB

In all the cases that the lift force is bigger with respect to the Dean drag force, it can be concluded that the particles will stay focused at the inner wall.

A structural mesh is created by using the software POINTWISE putting 51x51 nodes for each cross section (50x50 cells for each cross section).

The values of cells are these:

Exported from Pointwise V18.4R4

2863701 nodes.

2750000 hexahedral cells, zone 2.

8137500 quadrilateral interior faces, zone 3.

2500 quadrilateral velocity-inlet faces, zone 4.

2500 quadrilateral pressure-outlet faces, zone 5.

220000 quadrilateral wall faces, zone 6.

Increasing the number of cells implicates a higher computational time but there will be a lower residual in the simulation.

The coordinate of the center of the inlet surface,in mm, is (-0.569, 0, 0.761). Given that the problem is symmetric with respect to the axis of the channel (the velocity that there is to the left of the axis is equal to the right), at least 51 nodes at the height edge (50 cells) of the cross section are needed to see the fluid dynamics (Dean vortex and so the shift of the velocity on the external curvature). A very thick mesh on the direction of the flux is not needed because it is only a simple Poissel flow and so a high aspect ratio is used but not too high because there may be the issue of tracking particles. The first thing done was to check if the scale of the spiral is correct, then the setting process may commence.

The "multi phase" model must be turned off because as multi phase ANSYS means Eulerian phase and in this problem case, there is one Eulerian phase (water) and the particles must be studied with a Lagrangian approach.

A transient time is used.

A Discrete phase is used, enabling the interaction with continuous phase, this means that there is a 2 way coupling and so that particle motion is affected by the fluid and vice versa. It is very important to increase the "max number of steps", because the particles need a certain time to exit. As a physical model it has enabled the Saffman lift force and the rotation of particles and so the Magnus force is not considered.

As time step of calculation it was used 0.001 second.

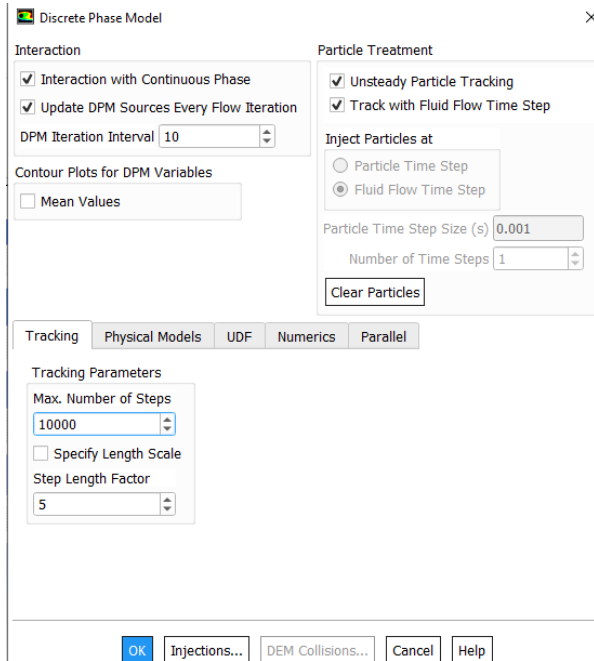


Figure 4.20: ANSYS setting in DPM

As injection type there are two different ways:

- 1)single injection
- 2)surface injection

4.3.1 Single injection

The goal is to inject 7 particles inside the domain.

The ratio of particle diameter and hydraulic diameter was calculated to see if the particles are well focused or not:

Table 4.1

	$\frac{a}{D_h}$
$a=7\mu m$	$0.1049 > 0.07$
$a=10\mu m$	$0.1499 > 0.07$
$a=15\mu m$	$0.2249 > 0.07$
$a=20\mu m$	$0.30 > 0.07$

It was conclude that all the particles, independent from the size, are balanced at the inner wall. The Stokes number eq.(3.22) was calculated to verify that was much less the 1, in such a way the particles are able to follow the path line.

If a particle with a diameter of $20\mu m$ is used, a tracking problem will occur.

Table 4.2

u[m/s]	d _p [m]	m _p [Kg]	t _p [s]	St _p
0.01667	7E-6	1,88574099e-13	2,84978e-06	0,000712553
0.01667	10E-6	5,49778714E-13	5,81589E-06	0,00145419
0.01667	20E-6	4,39822972E-12	2,32635E-05	0,005816758
0.1667	7E-6	1,88574099e-13	2,84978e-06	0,007125529
0.1667	10E-6	5,49778714E-13	5,81589E-06	0,014541895
0.1667	20E-6	4,39822972E-12	2,32635E-05	0,05816758
0.2667	7E-6	1,88574099e-13	2,84978e-06	0,011399991
0.2667	10E-6	5,49778714E-13	5,81589E-06	0,023265287
0.2667	20E-6	4,39822972E-12	2,32635E-05	0,09306115

The particle diameter used in this simulation is $7\mu m$ and the velocity inlet of the solution is $0.1667 m/s$ that corresponds to a mass flow rate of $50\mu l/min$.

The mass flow rate was calculated in such a way that 1 parcel correspond to 1 particle. The mass of the single particle is $1.88574099 \cdot 10^{-13}$ and using the eq.(4.11) the result value is $1.88574099 \cdot 10^{-10}$. 0.001 was used as start time of injection in such a way to lower the residual and since 1 particle each 0.001 second is injected, the stop time is 0.008.

The particles were injected from the center of the inlet surface with a 0 velocity. When the particle is injected, a small offset to the injection surface is needed because the particle is not able to enter in the domain.

The results obtained in the simulation show that the particles in the first arc of the spiral have a uniform distance and are able to follow the streamlines of the fluid, as can be seen in Figure 4.21 and 4.22.

Due to the fact that there is the Dean force, they are shifted to the external wall and since FLUENT does not have the wall lift force, the particles are stacked against the wall and remains there because the Saffman lift force is not so big, as it has shown in Figure 4.23.

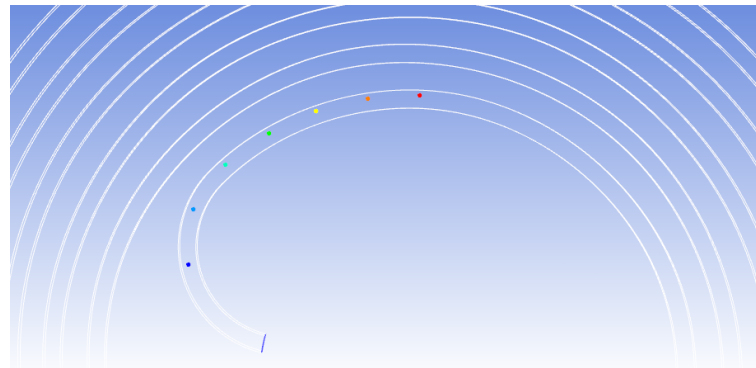


Figure 4.21: injection of particles

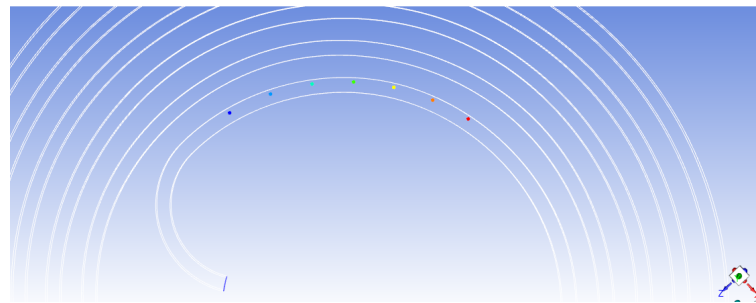


Figure 4.22: the particles are following the stream line

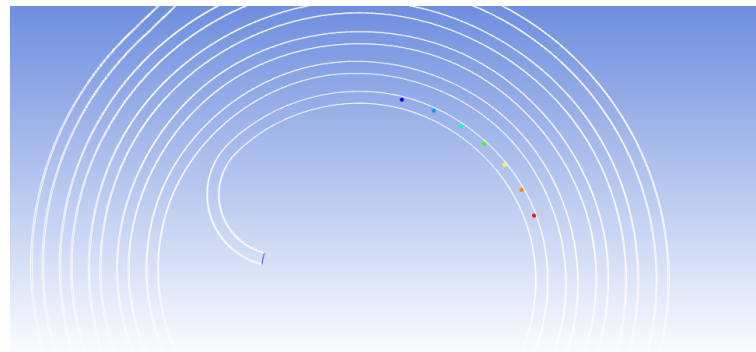


Figure 4.23: particles crashed against the external wall

In all these results the particles are not shifted to the inner wall because FLUENT does not include the inertial lift force and so only the effect of the Dean force that pushes the particles to the external wall is visualized.

4.3.2 Surface injection

"Surface" released from inlet was used, in this way the parcels are injected from the inlet surface and each one is arranged in one cell of the surface. Since that the cross section mesh is composed of 2500

cells, there 2500 parcels will be injected.

A particle diameter of $7\mu m$ was used, a start time of 0.001 second and a stop time of 0.002 second (instantaneous injection) was set, that correspond to the time in which the injection of the particles is stopped and this time coincide with the single step time of the simulation. The particles have an initial velocity equal to the fluid.

To calculate the mass flow rate, the eq.(4.41) is used, where the mass of the single particle is $1.88574099 \cdot 10^{-13} kg$ and the number of particles is 2500.

The result is $4.714352475 \cdot 10^{-7} kg/timestep$.

Basically, 2500 parcels correspond to 2500 particles and in this way the correct particle tracking can be seen.

The Reynolds particle number from eq.(26) is 0.1219.

The net inertial lift force is $7,48962 \cdot 10^{-18} N$.

From the eq.(2.1) the channel Reynolds number was calculated and is 11.0579. The Dean number calculated from eq.(2.19) in the loops drawn and the corresponding Dean force eq.(2.21) are the following:

D_h starting loop	D_h 1°loop	D_h 2°loop	D_h 3°loop	D_h 4°loop	D_h 5°loop
1.777537319	1.116451101	1.061107288	1.01453256	0.972467167	0.935234726
<hr/> <hr/>					
F_{Dean} starting loop	F_{Dean} 1°loop	F_{Dean} 2°loop	F_{Dean} 3°loop	F_{Dean} 4°loop	F_{Dean} 5°loop
3.04192E-11	1.42535E-11	1.31199E-11	1.21943E-11	1.1381E-11	1.06793E-11

Table 4.3

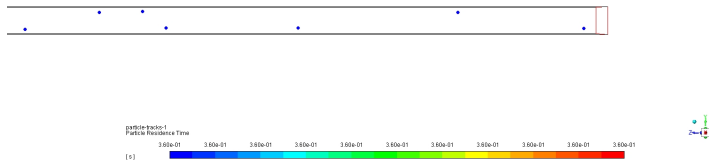


Figure 4.24: outlet lateral view of the straight channel

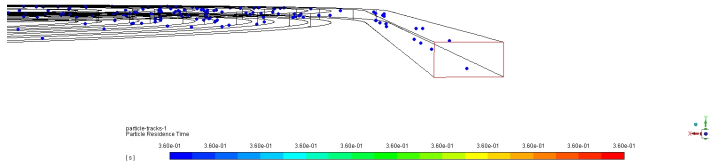


Figure 4.25: outlet 3D view of the straight channel

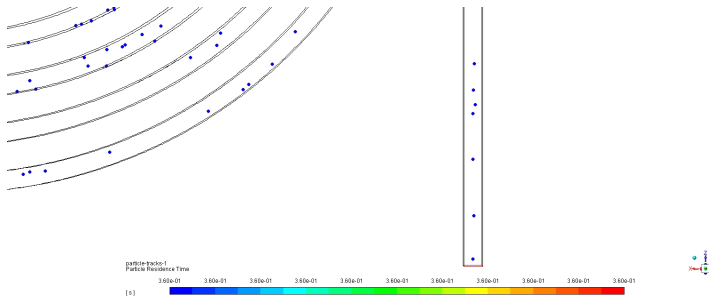


Figure 4.26: outlet upper view of the straight channel

When a lot of particles are injected, it can happen that some particles remains stuck to the external wall and others are able to win the force and can continue the trajectory. The Dean force pushes the particles toward the external wall where there will be the vortexes that push the particles toward the internal wall. Since there is no the net lift force, there will not be an equilibrium of the particles and they will oscillate between the internal and the external walls forever.

Chapter 5

UDF IMPLEMENTATION AND FINAL RESULTS

5.1 Numerical method for lift force

The equation of the lift force obtained by Asmolov considers the particle as a point.

The numerical method considers a rigid sphere with diameter a suspended in a rectangular straight pipe and a Poiseuille flow.

The origin of the coordinate system is located at the center of the channel inlet surface.

The lift force can be written as a function of:

$$F_L = f(a, y, z, H, W, U_{max}, \mu, \rho_f) \quad (5.1)$$

Using the Buckingham theorem, from the 8 parameters 5 dimensionless parameters are obtained using U_{max}, H, ρ_f to dimensionless them.

$$F_L = f\left(\frac{a}{H}, \frac{y}{H}, \frac{z}{H}, 1, \frac{W}{H}, 1, \frac{\mu}{\rho_f U_{max} H}, 1\right) = f(\kappa, y^*, z^*, AR, Re) \quad (5.2)$$

A particle located at different lateral positions (y^*, z^*) will experience different hydrodynamic forces from the ambient flow that changes the lift force in magnitude or direction.

5.2 Simple straight channel test

When the fluid is injected from the inlet surface of the pipe, FLUENT will give a flat velocity profile at the inlet.

After a certain length due to the fact that there is the no slip boundary condition at the wall and the fluid is real (the viscosity is different from 0), the profile will become parabolic.

The max velocity that will be reached (center of the pipe) it is different from the inlet velocity that

was imposed at the inlet surface.

In Figure 5.1 a straight pipe can be seen, as the flow developed, the velocity gradient at the wall reduces.

There is a pressure drop from inlet to outlet that can be estimated from the equation of Darcy-Weisbach.

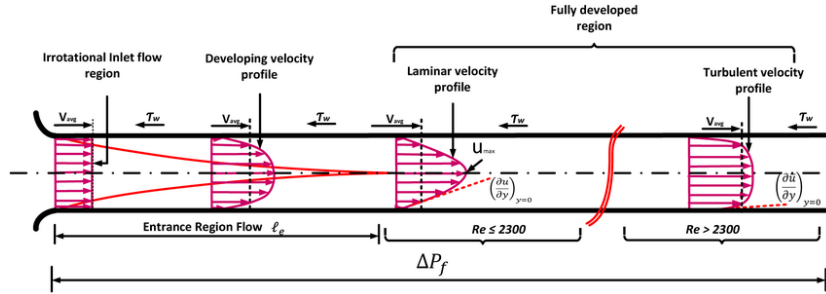


Figure 5.1: developing of the parabolic profile inside a pipe

When particles are injected slightly shifted from the center of the pipe, they will feel the shear gradient lift force due to parabolic profile.

To see this effect the fully developed flow region must be achieved and then the particles will be shifted toward the channel walls.

Due to the fact that FLUENT does not include the wall lift force the particles remain stuck to the wall.

This force can be added with a UDF.

The lift coefficient cannot be calculated for particles that have real diameter but was calculated theoretically by Schonberg Hinch for $a/D_h = \kappa \ll 1$ and $Re = 15$ and it was seen that there is not significant difference considering the particle as a point mass, as can be seen in Figure 5.2, where y is the y coordinate position of the particles.

The experimental results are correct with the eq.(2.16), in fact when κ increases, the lift coefficient decreases.

The curve shown in Figure 5.4 can be obtained using INVENTOR and plotting all the x and y data of the function, then with MATLAB it is possible to calculate the curve by doing a polynomial approximation.

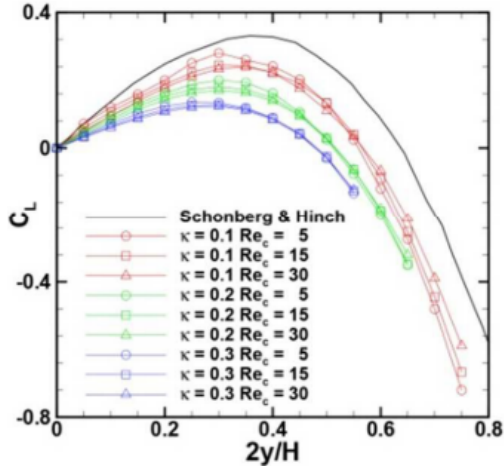


Figure 5.2: the following picture shows the graph of the lift coefficient for different values of Re and k

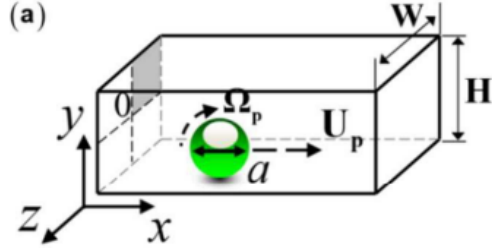


Figure 5.3: the following picture shows the particle inside the channel

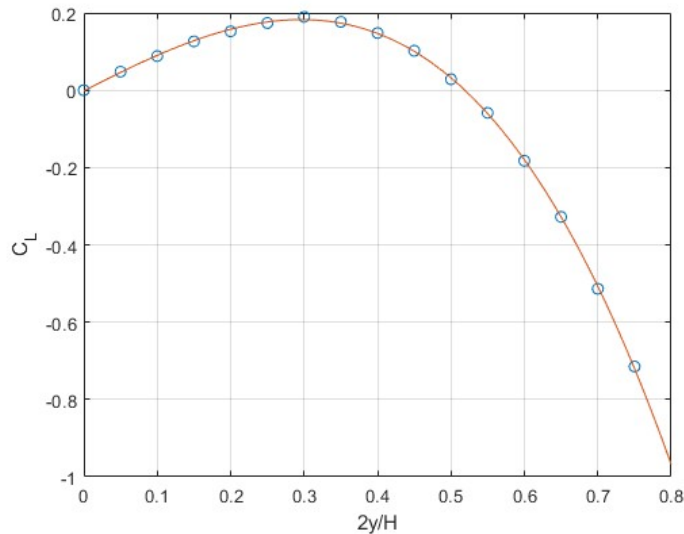


Figure 5.4: plot of the lift coefficient along y axis using MATLAB

The coefficients of the polynomial are the following:

$$C1 = -3.0374; C2 = -0.3046; C3 = 0.9790; C4 = -0.0016;$$

This equation is valid only for $z=0$.

If the particle is a little bit shifted from the center axis they will feel the shear gradient lift force and when $2y/H = 0.63 - 0.64$ the equilibrium between shear and wall lift force occurs.

It was seen that the lift coefficient increases linearly with $2z/H$, and then decreases rapidly due to wall lift force, when it is closed to the channel center, as can be seen in Figure 5.5.

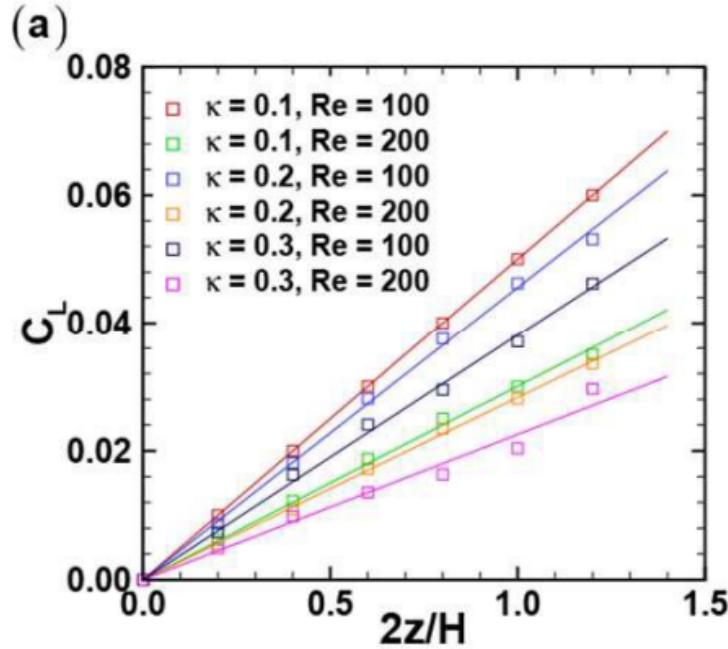


Figure 5.5: trend of the lift coefficient in z direction for different values of Re and k

Far from the center line of the channel, the lift coefficient profile is completely different.

In this experiment, Figure 5.6 the red curve represents the lift coefficient calculated at the center axis of the channel and the green curve is for $2y/H = 0.6$, both calculated for AR=0.5 and Re=100.

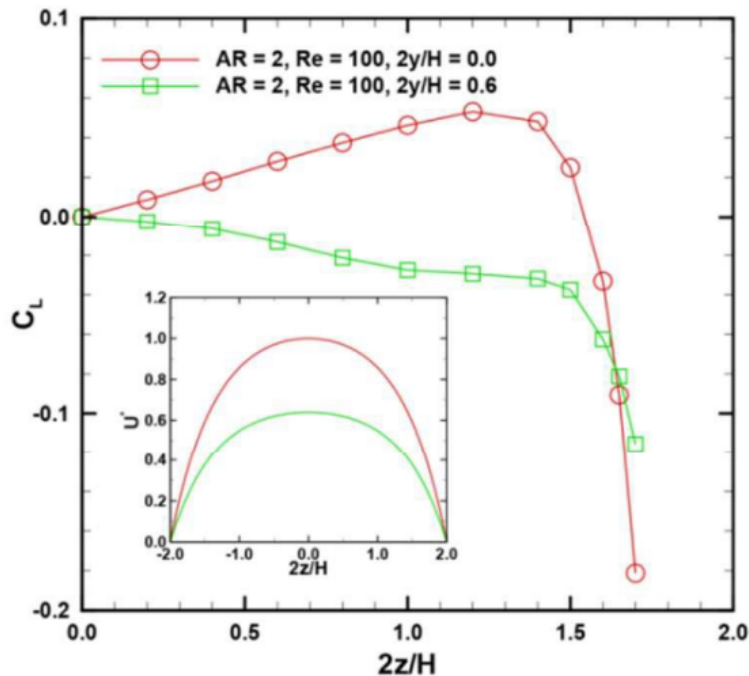


Figure 5.6: lift coefficient along the z axis for a certain fixed y position

The lift coefficient can be modeled with the following piece wise equation:

$$(5.3) \quad \begin{cases} \frac{0.047-\gamma}{1.2} \frac{2z}{H} & \frac{2z}{H} \in (0, 1.2) \\ 7.3046 \cdot (\gamma - 0.127) \left(\frac{2z}{H} \right)^2 - 17.531 \cdot (\gamma - 0.127) \frac{2z}{H} + 9.51863 \cdot (\gamma - 0.135405) & \frac{2z}{H} \in [1.2, 1.8) \end{cases}$$

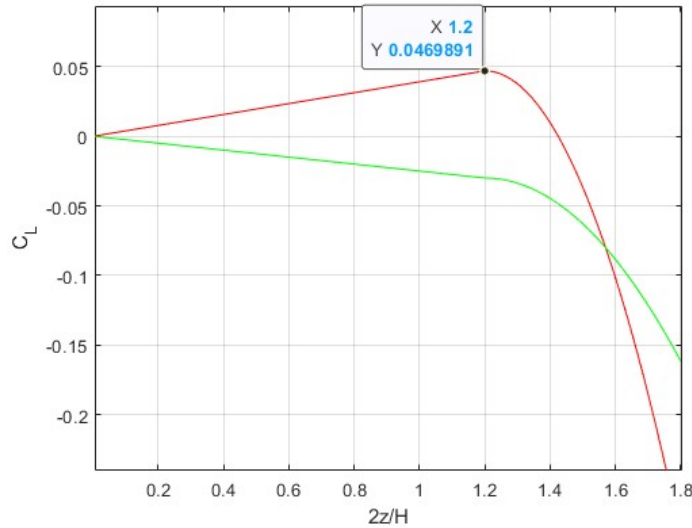


Figure 5.7: plotting the piece wise equation

Where $\gamma = \frac{2y}{H} \cdot \frac{0.077}{0.6}$. When moving in the positive value of the $2z/H$ axis, it can be observed a linear increment and a suddenly parabolic decrements of the function C_L . This law is a function that depends on the point of the axis $2y/H$ in which it is located.

In Figure 5.8 is plotted the vector field of C_L where along the z axis there is the vector field that follow the function of two variables and along the y axis there is the vector field that follow the law of the cubic polynomial.

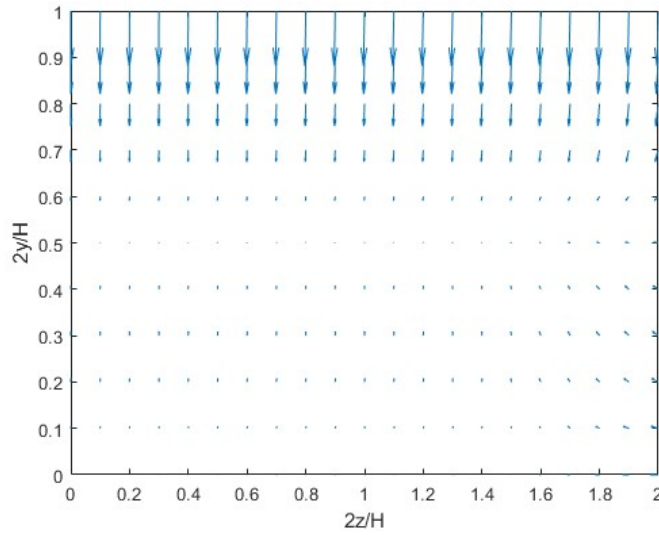


Figure 5.8: vector field of lift coefficient in the first quadrant of the cross section

5.3 Particles focusing in a straight channel

In this numerical modeling it was studied the focusing of the particles in a straight channel.

The coordinate system of the domain is located at the center of the initial cross section as can be seen in Figure 5.9:

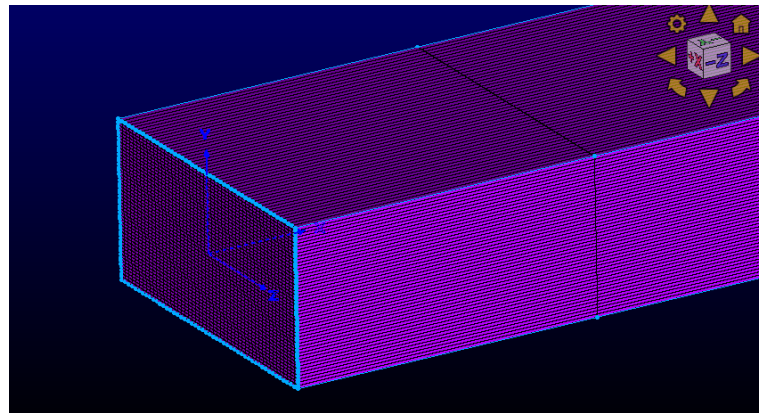


Figure 5.9: 3D mesh of the straight channel

The channel has a rectangular cross section with $W=0.1\text{mm}$ and $H=0.05\text{mm}$.

A single injection of particle was done from $(0,-0.02,-0.045)$ and $(0,0.02,0.025)$ as shown in Figure 5.10:

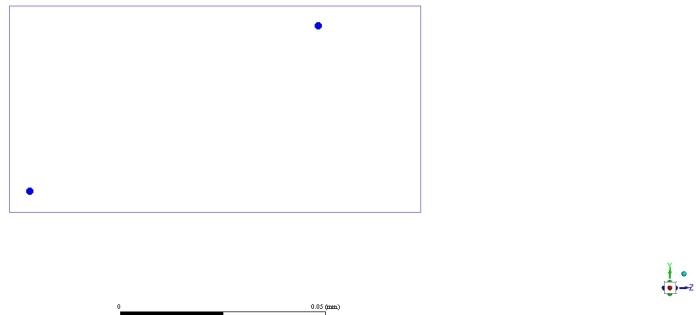


Figure 5.10: inlet position of particle in the cross section

A UDF was applied to take into account the shear gradient lift force and the wall lift force.

The code can be found in the APPENDIX A.

After some length the particles will be focused in two lines up and down as is known from the theory and the result is shown in Figure 5.11.

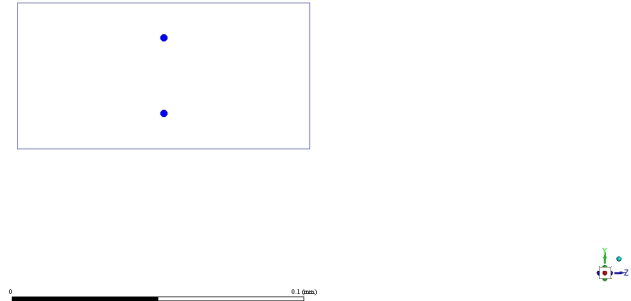


Figure 5.11: equilibrium position of particles in the cross section at the end of the channel

5.4 General UDF for different channel shape

In the previous UDF, the particle position was referred respect to the coordinate system replaced a the inlet cross section surface.

This can be a problem for 2 reasons:

- 1)if spiral channel is used, because the z and x direction changes every time and the force is not in the correct direction;
- 2)since that the particle distance respect to the wall is needed, this cannot be done.

A UDF that is independent from the coordinate system was built and the particle wall distance was calculated respect to the wall and not respect to coordinate system.

To calculate the particle wall distance (minimum distance) fluent does not have a function and so

one it was built.

In Figure 5.12 is shown a particle (red dot), this particle will have a position respect to the coordinate system (position vector in red). To find its distance (minimum distance) respect to the upper wall all the centers of the upper wall face (blue dots) are taken and green vector is obtained, that is the position vector of the center face. Doing the subtraction of these two vectors, the gray vector, that is the particle wall distance vector is obtained. Doing a for cycle of all blue dots in the upper wall, the minimum distance can be found.

This minimum distance is not orthogonal with the wall and so it was created a normal vector placed at the node centroid that as been found the min distance and the dot product of the grey vector time orange normal vector is done.

In this way it is found the distance that is independents from the coordinate system and so it is possible to use any shape channel.

The same result can be obtained if another wall is take to calculate the particle distance.

To get a correct value of particle position the residual should go below 10^{-4} .

If a force on the particle is applied, due to wall lift and shear gradient the particle should change its position.

In discrete phase model the DPM iteration is set to 10, this means that since one time step is composed of 0.001 second, with a max number of iteration equal to 20, FLUENT will calculate the distance 2 times in this time step. The correct value is at the end of the time step, because at iteration 10 some oscillations can appear.

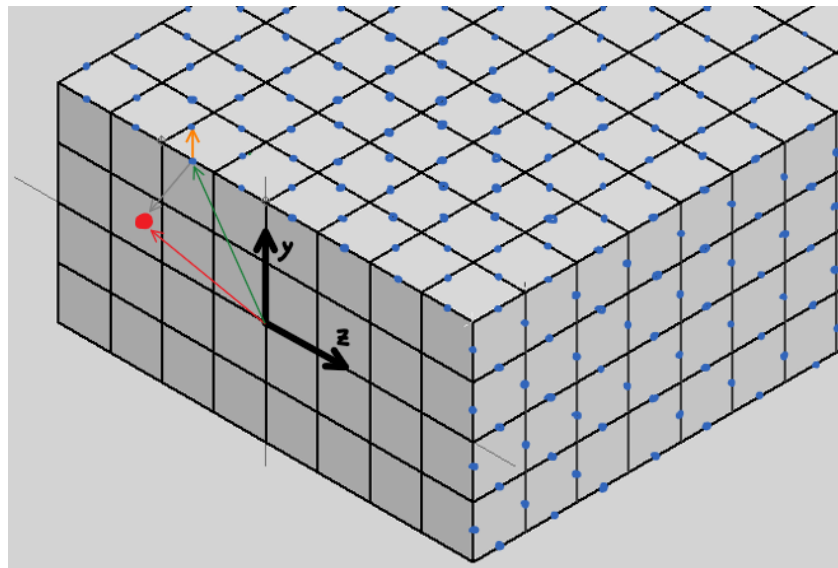


Figure 5.12: vector distance of the particle with respect to the upper wall with ID=9

The important thing in this UDF is that the y axis must point up, and the cross section is in the plane YZ as can be seen in Figure 5.12.

A square, rectangular or trapezoidal cross section can be used.

The DPM body force UDF works in this way:

the function wants as input p and i, where p is the particle pointer and i is an index that can be 0,1 or 2 and corresponds with the geometrical axis.

FLUENT will enter in the UDF 3 times, one time for 0 where it compile all the UDF and only the i=0 condition and calculates the F_x force, the second time for 1 and at the end with 2.

It is very important to use the index i only in the force condition and not for other cases in the code because if FLUENT finds that index it will put only one value 0,1 or 2 and a wrong result can be obtained.

When a message is printed in the console of FLUENT (e.g. the value of the force in three directions) is it possible to have more than 3 messages. Each parcel has its position checked every time it moves. That is typically on entering a cell, 1-2 time in the cell and on leaving. In transient 500 particle (default) are got, sub steps per time step, in steady it is 5000 (which often is not enough). So, each particle will generate up to 500 messages per time step, or 5000 per track. It will get up to 1000 per time step, with up to 500 per DPM update (since that is a time step there are 20 iterations and only 2 DPM iterations each 10 iterations). With the accuracy control tools the number of steps may be reduced if the particles are not changing direction very much.

The UDF will be called for each particle that are in the domain.

If there are two DPM iterations, at the second DPM the particle position will be changed again to reach at the end of it the convergence of correct position. The best thing to do if a collect data wants to be done, is to set DPM iteration only ones at each 20 iterations, in this way there will not be any changes.

The UDF can be found in the APPENDIX B.

To validate this UDF, a data file from FLUENT was collected, where is printed the lift coefficient in a straight channel.

The particle was injected at $2y/H = 0.5$ and the particle was very close to the lateral wall in such a way to have a big range of the domain of the function.

The result that has been obtained is nice and there is an overlapping of curves.

In Figure 5.13 can be seen that the curve stopped before because the particle was already out.

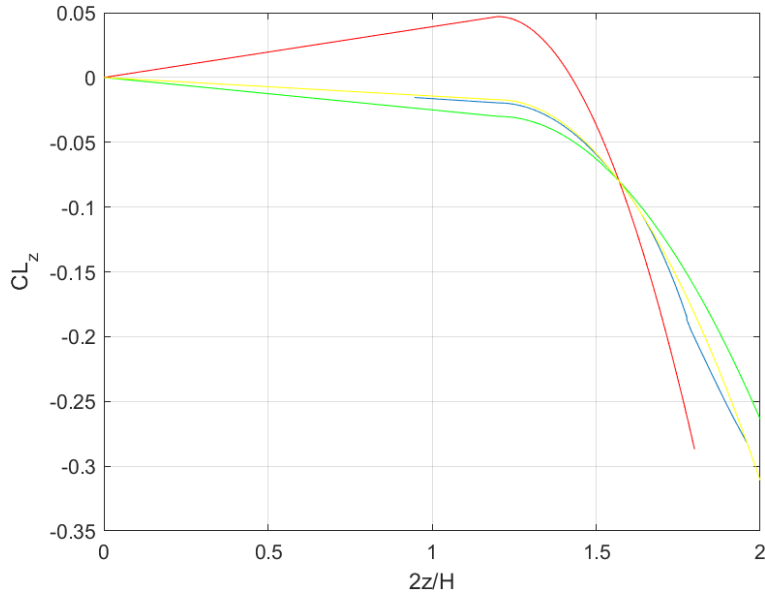


Figure 5.13: the blue curve represented the lift coefficient graph obtained from FLUENT that is equal to the yellow curve obtained fro the piece wise equation

As can be seen the yellow curve is for $2y/H = 0.5$ and the blue one is the curve obtained from data.

5.5 Results of spiral channel with rectangular cross section

In the following section the general UDF was applied for a spiral composed by 4 loop, the spiral is the same of the simulation that was done without UDF.

4 particles with diameter of $20\mu m$ were injected with random position in the inlet cross section.

The mass flow rate was $80 \mu l/min$ that correspond to a velocity of $0.2667 m/s$.

The particles are injected with initial velocity equal to the fluid at the same time and as can be seen in Figure 5.14 in the initial loop, the Dean force is high and the particles are shifted to the external wall.

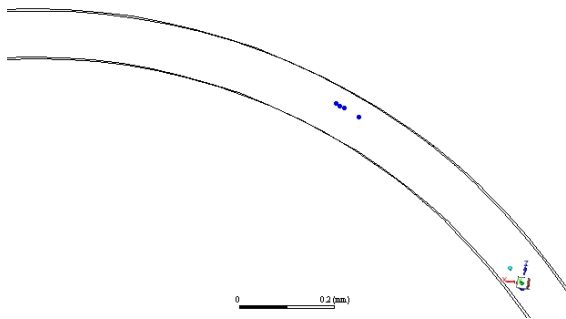


Figure 5.14: starting loop

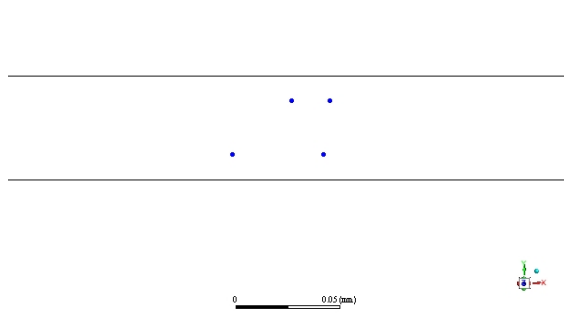


Figure 5.15: starting loop

The distance between particles in the 3°loop is $86\mu m$ in the x direction and $25.6\mu m$ in the y direction.

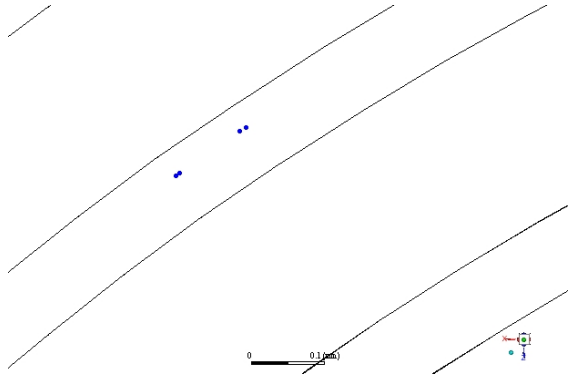


Figure 5.16: 3°loop

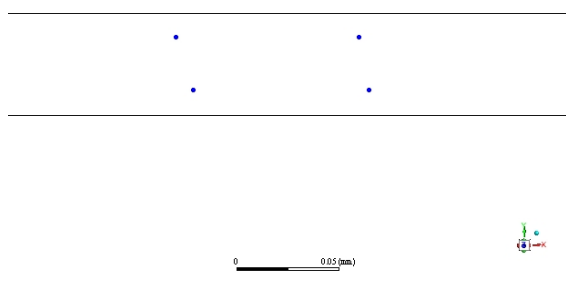


Figure 5.17: 3°loop

The distance of the particles respect to the wall in $11.5\mu\text{m}$.

The following Figure 5.18, is an experiment done with a mass flow rate of $15\mu\text{l}/\text{min}$.

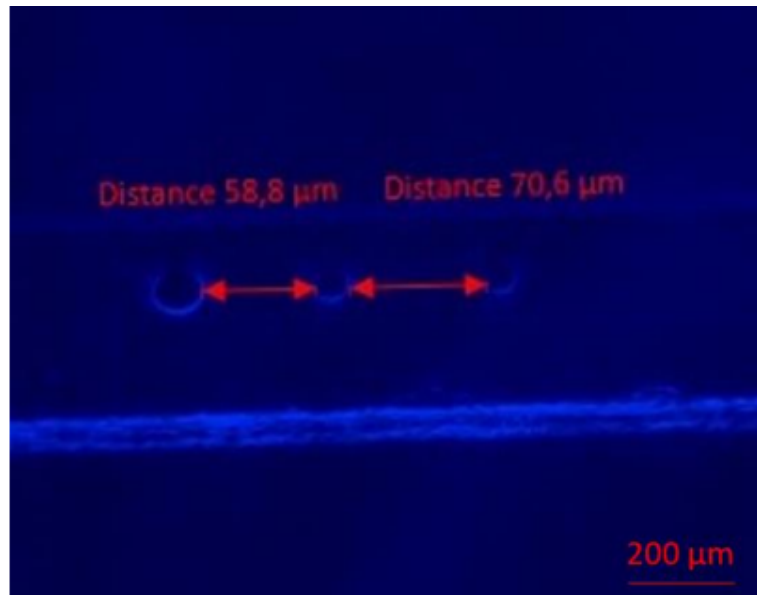


Figure 5.18: real result of particle focusing in a spiral channel

As can be seen from the simulation, the particles are focused at the outer wall but this is a wrong result because from the literature the particles must focused at the inner wall.

The only reason is that the function of the net lift force is not correct for that initial condition of inlet and cross section dimension of the spiral.

5.6 Improvement of the model

Also CL_y is a function of two variable $2y/H$ and $2z/H$.

In the previous model was not put the dependency of $2z/H$.

In Figure 5.19 it is shown the y lift coefficient obtained for $Re = 125$, aspect ratio of 0.6667 and

$k = 0.2$.

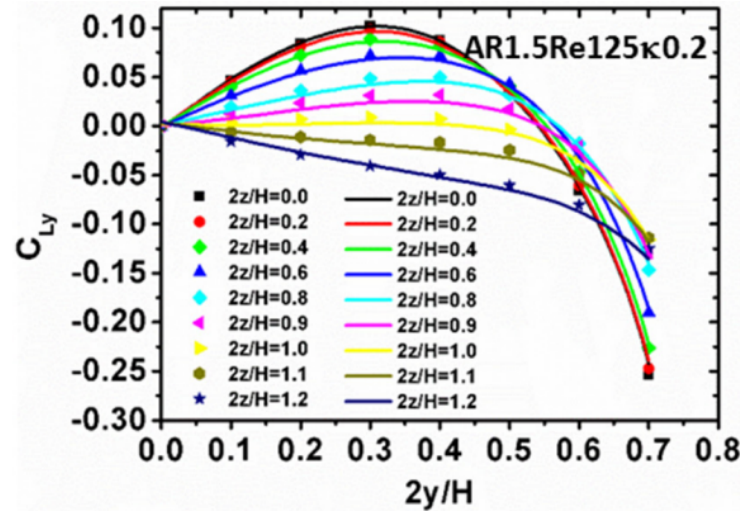


Figure 5.19: trend of the lift coefficient over $2y/H$ axis for a fixed $2z/H$

To obtain that function MATLAB was used, importing all the data and generating a polynomial function of degree 3 for x and degree 5 for y, doing fitting.

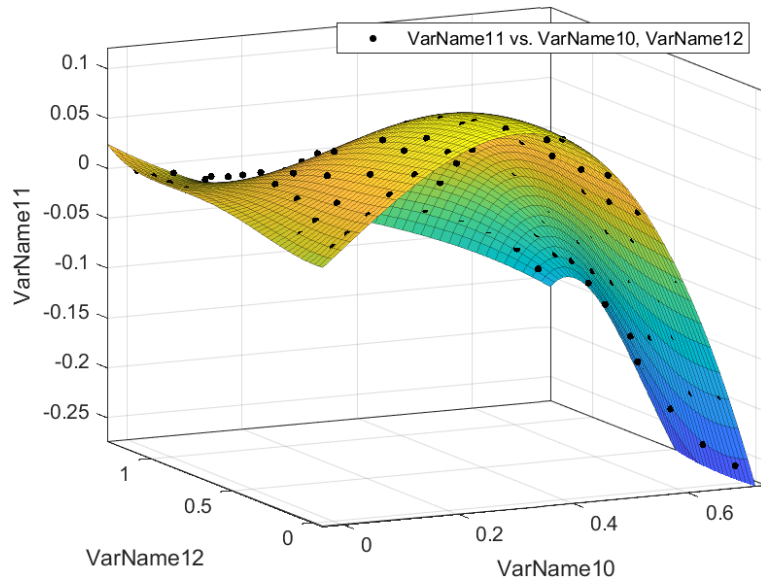


Figure 5.20: fitting of CL_y

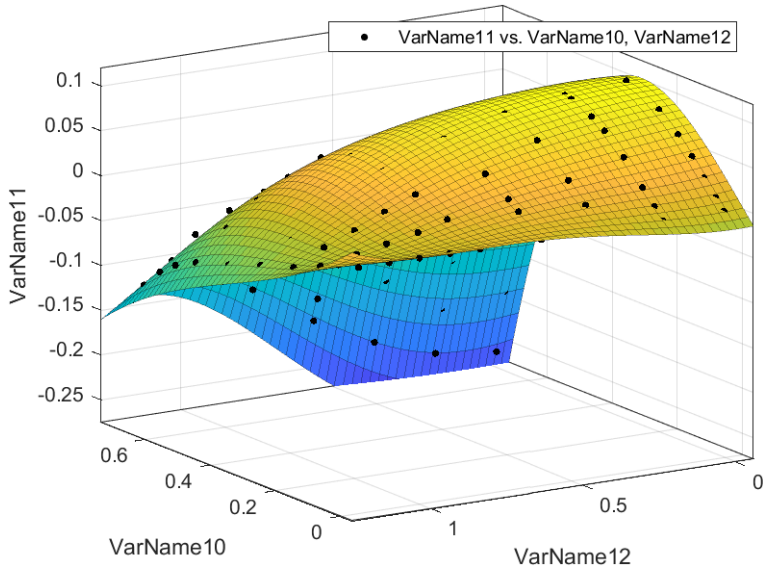


Figure 5.21: fitting of CLz

Where in Figure 5.20, on the z axis (variable 11) is represented the output that is CL_y , on the x axis (variable 10) there is $2y/H$ and on the y (variable 12) there is $2z/H$.

As can be seen, it was obtained a function of two variables (surface) that better approximates all the points data.

The function is the following:

$$CL_y = p_{00} + p_{10} \cdot x + p_{01} \cdot y + p_{20}^2 + p_{11} \cdot x \cdot y + p_{02} \cdot y^2 + \\ p_{30} \cdot x^3 + p_{21} \cdot x^2 \cdot y + p_{12} \cdot x \cdot y^2 + p_{03} \cdot y^3 + p_{31} \cdot x^3 \cdot y + \\ p_{22} \cdot x^2 \cdot y^2 + p_{13} \cdot x \cdot y^3 + p_{04} \cdot y^4 + p_{32} \cdot x^3 \cdot y^2 + p_{23} \cdot x^2 \cdot y^3 + p_{14} \cdot x \cdot y^4 + p_{05} \cdot y^5 \quad (5.4)$$

where the following are the coefficients of the polynomial:

$$p_{00} = 0.0011; p_{10} = 0.4649; p_{01} = -0.01504; p_{20} = 0.1066; p_{11} = -0.402; p_{02} = 0.1195; \\ p_{30} = -1.803; p_{21} = 2.221; p_{12} = -0.8143; p_{03} = -0.1319; p_{31} = -2.416; p_{22} = -0.6427; p_{13} = 1.06; \\ p_{04} = -0.02916; p_{32} = 2.788; p_{23} = -0.7275; p_{14} = -0.4391; p_{05} = 0.05612;$$

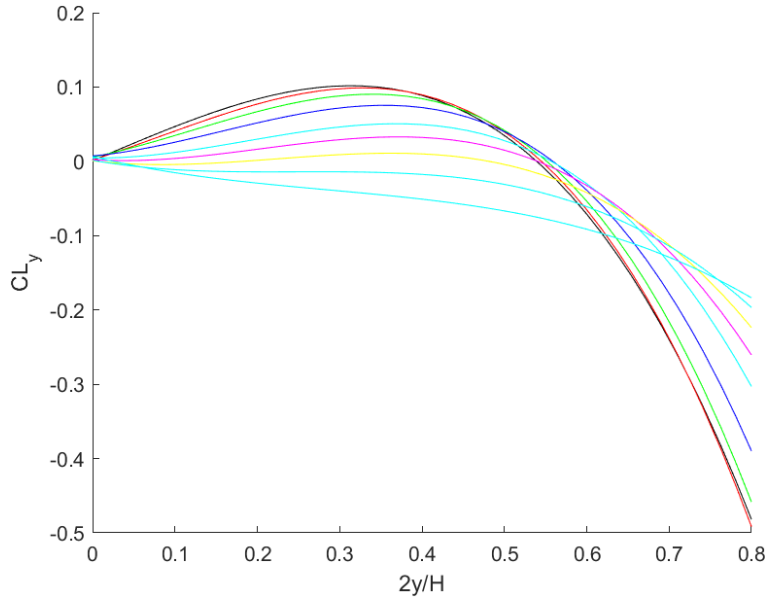


Figure 5.22: 2D plot of the Figure 75

5.7 Simulation of 3 loops spiral channel with AR=0.5, Re=100 and k=0.1

In the following section it was simulated a rectangular cross section channel with an aspect ratio of 0.5, a Reynolds number of 100 and a ratio of particle diameter and small edge channel of 0.1.

A particle with diameter $a = 10\mu m$ was used and from k was possible to calculate H that should be equal to $0.1mm$.

Since that $AR = 0.5$, $W = 0.2mm$ was obtained.

The hydraulic diameter calculated is $D_h = 0.13333mm$.

Since that a $Re = 100$ is required, a mass flow rate of $Q = 900\mu l/min$ must be used, that correspond to an initial velocity of $0.75m/s$.

The Dean number calculated at the last loop considering the inner wall is 7.61.

In Figure 5.23 it is shown the geometry of the spiral:

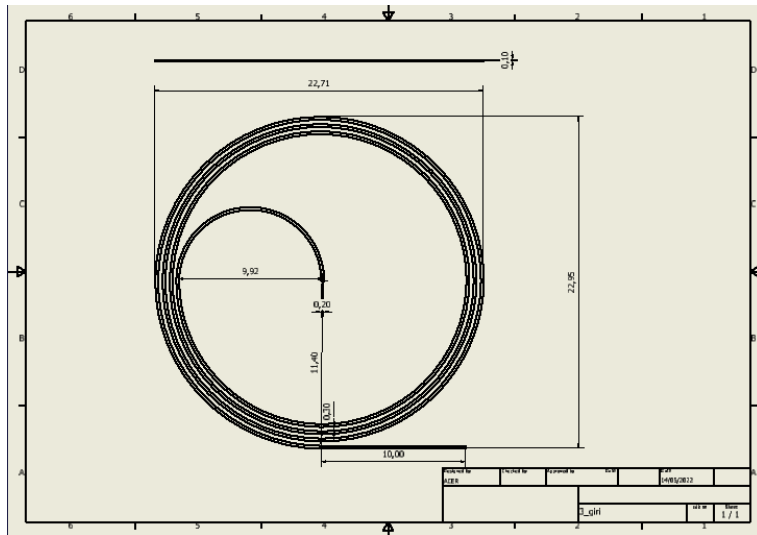


Figure 5.23: geometry of the spiral

The model for the lift coefficient was imported. The model is very sensible to the initial condition of Re , k and AR and changing these 3 there will be different curves.

In this case the function is the following:

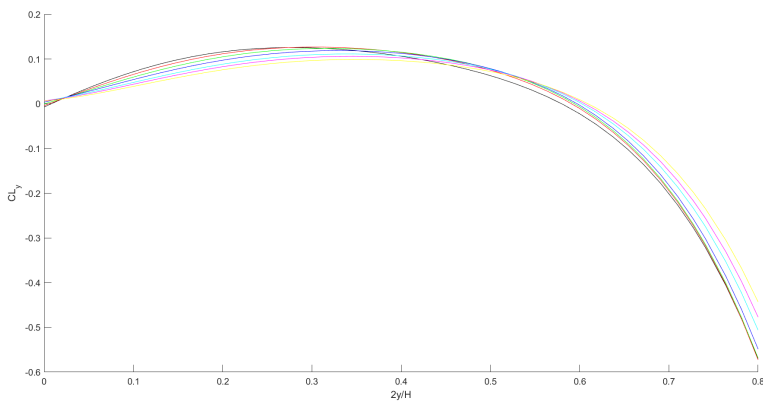


Figure 5.24: plotting of the CL_y over $2y/H$ for a fixed $2z/H$

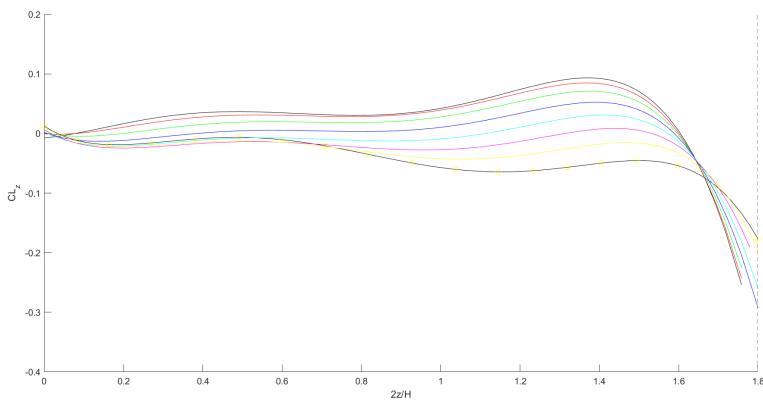


Figure 5.25: plotting of the CL_z over $2z/H$ for a fixed $2y/H$

These functions are obtained from data fitting using a polynomial function of degree 5 both for $2y/H$ and $2z/H$.

In Figure 5.26 it is shown the vector field of the lift coefficient:

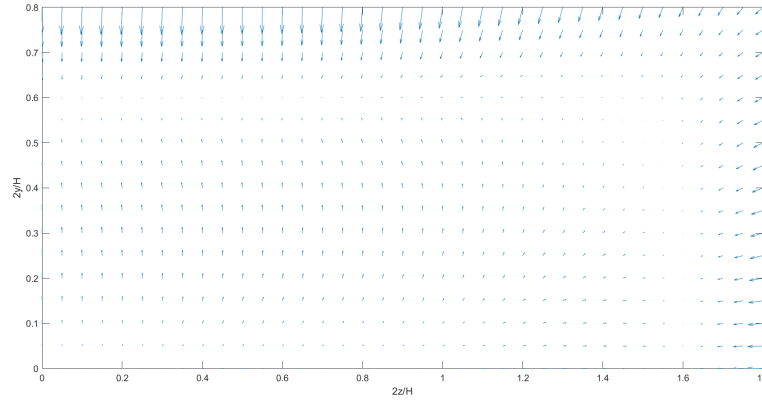


Figure 5.26: vector field of the lift coefficient

In Figure 5.27, it is shown the Dean vortex in the cross section calculated by FLUENT.

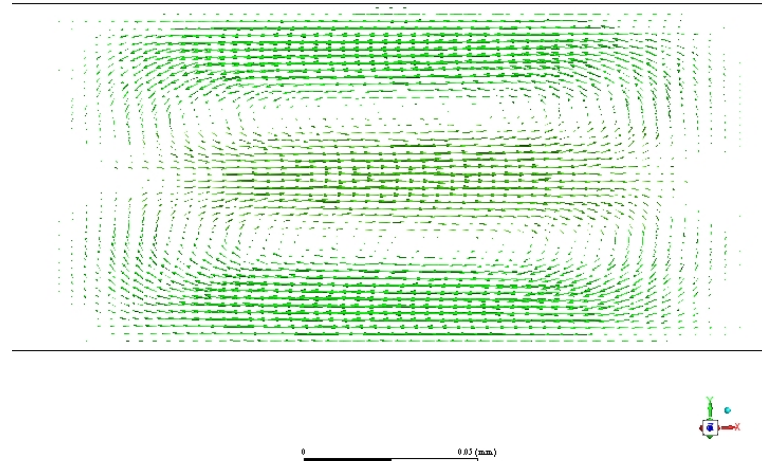


Figure 5.27: Dean vortex generated from the fluid dynamics

As can be seen in the previous Figure, the particles are pushed toward the outer wall due to dean forces and also due to centrifugal forces, when are close to that, they enter in the vortex that push the particles toward the inner wall. In this region the particles are balanced by the lift force and the dean force.

The centrifugal force is very high in the first arc of spiral.

10 particles are injected at random position as can be seen in Figure 5.28 and the focusing was obtained at the third loop as can be seen in Figure 5.32.

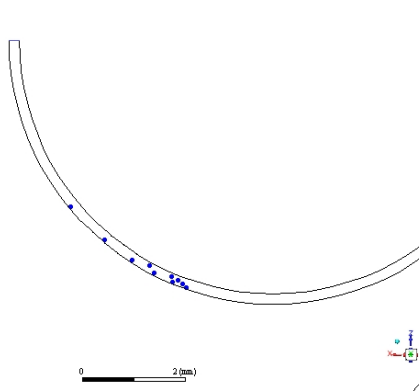


Figure 5.28: particles injected

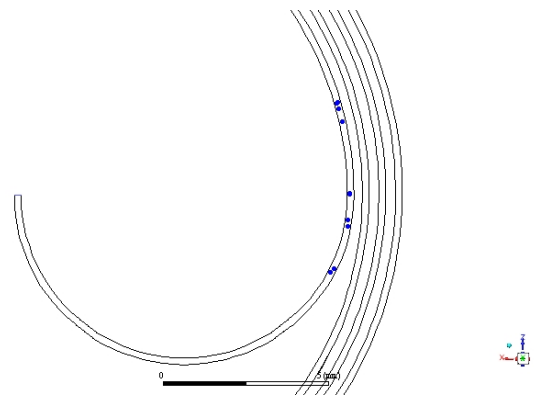


Figure 5.29: particles at starting arc

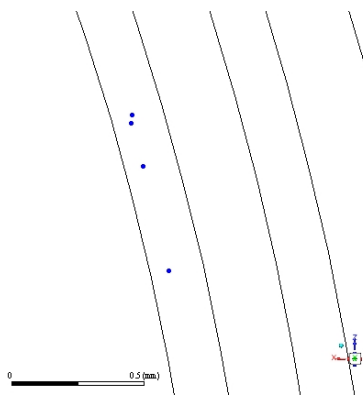


Figure 5.30: particles at 1°loop

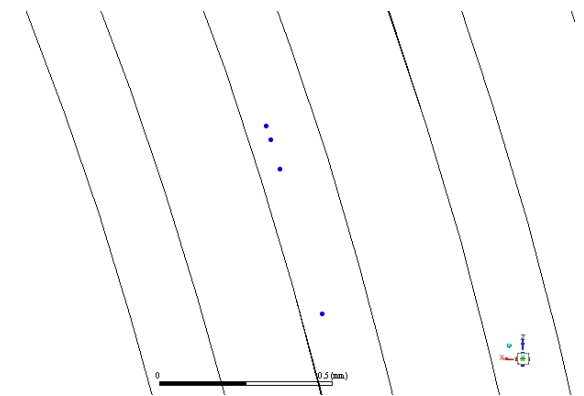


Figure 5.31: particles at 2°loop

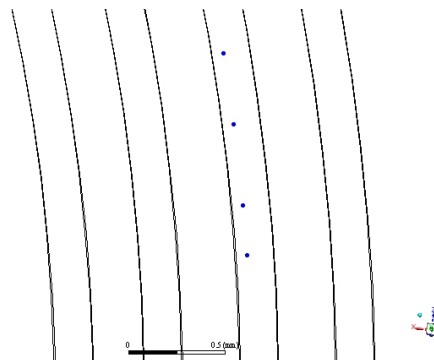


Figure 5.32: particles at 3°loop

In Figure 5.33 and 5.34 it is shown the lift coefficient in the z direction and y direction when the time grows.

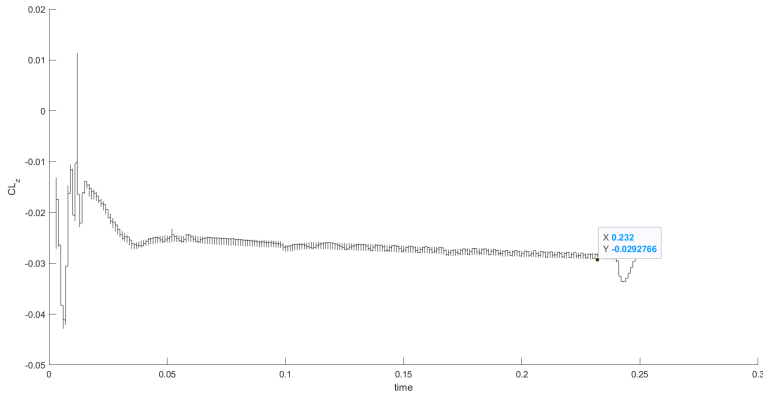


Figure 5.33: trend of CLz over time

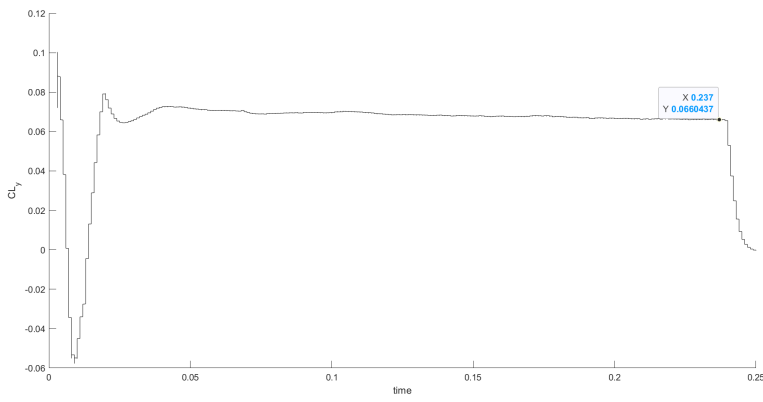


Figure 5.34: trend of CLy over time

In Figure 5.35, it is plotted the distance of the particle respect to the inner wall when the time grows.

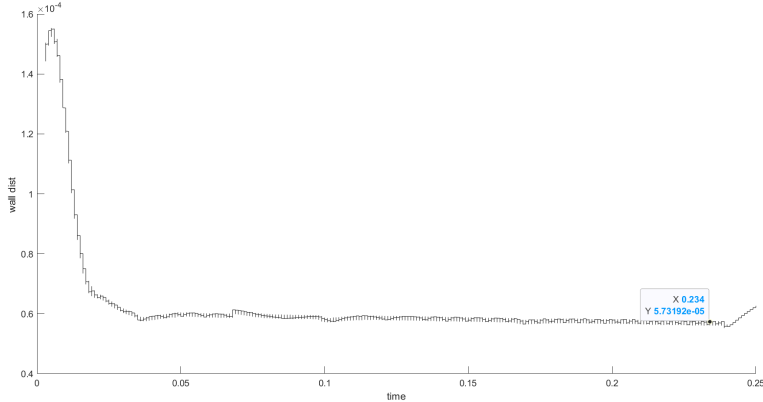


Figure 5.35: particle wall distance over time

In the first time the particle is very close to the outer wall and then due to Dean vortex it is close to the inner wall.

The distance of the particle is $57.32\mu m$.

As can be seen, when the particle reaches the straight channel, the distance of the particle with

respect to the inner wall increases because the focusing should occur at the center of the channel, as it is shown in Figure 5.36 and 5.37.

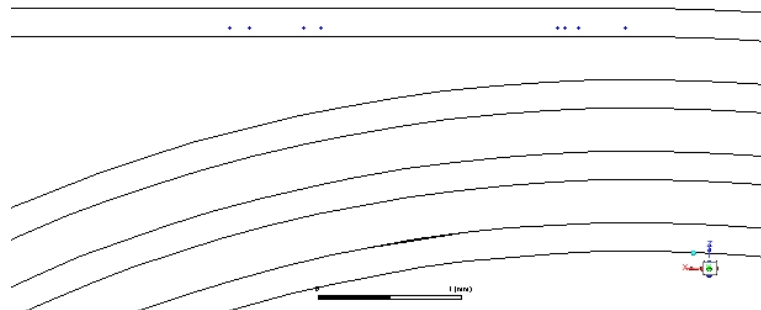


Figure 5.36: focusing of the particles at the end when the straight channel starts

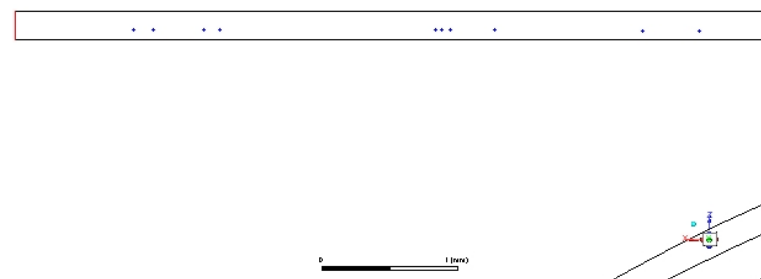


Figure 5.37: focusing of the particles at the end when the straight channel ends

In Figure 5.38 instead, it is shown the distance of the particle respect to the upper wall. If there are more particles, there will be the symmetric one.

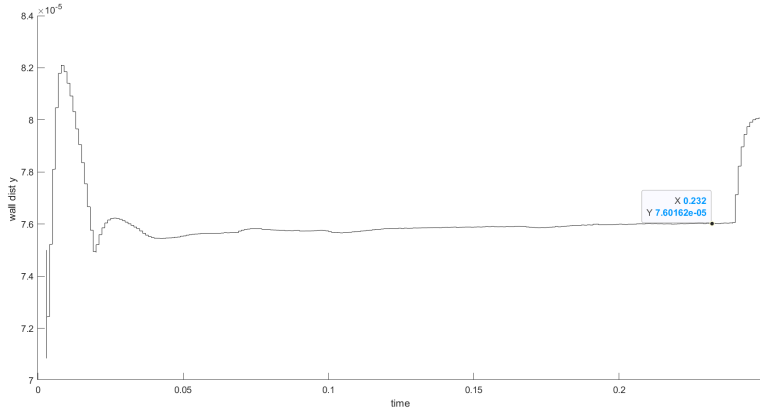


Figure 5.38: upper wall distance of the particle over time

The distance of the particle is $76.02\mu m$.

When the particle reaches the straight channel, the y distance of the particle increase ad this means that wants to go toward the center, but the focusing is not lost.

Now the simulation is correct because in the simulation was used the same Reynolds number, aspect ratio and particle diameter that it was used to build the net lift function.

5.8 Simulation of 3 loops spiral channel with AR=0.5, Re=50 and k=0.1

In this section, the spiral of the previous simulation was used but the Reynolds number was changed with $Re = 50$.

The mass flow rate is $450\mu l/min$ that correspond to an initial velocity of $0.375m/s$.

The Dean number is 3.81.

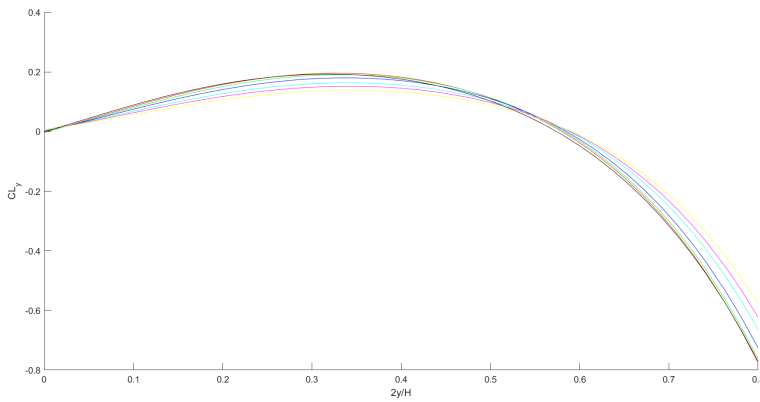


Figure 5.39: plotting of the CLy over $2y/H$ for a fixed $2z/H$

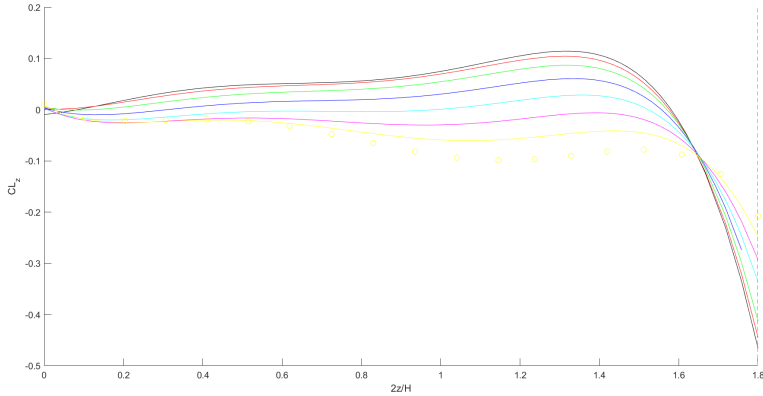


Figure 5.40: plotting of the CLz over $2z/H$ for a fixed $2y/H$

The results obtained are the following:

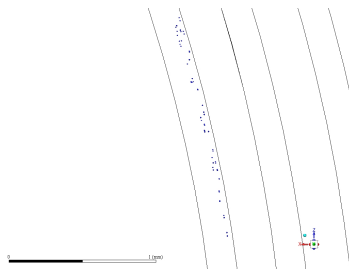


Figure 5.41: particles injected at starting arc

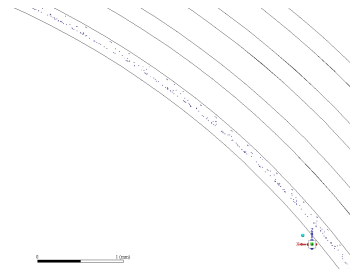


Figure 5.42: particles at 1° loop

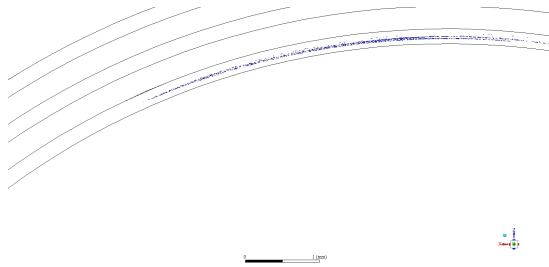


Figure 5.43: particles at 1° loop

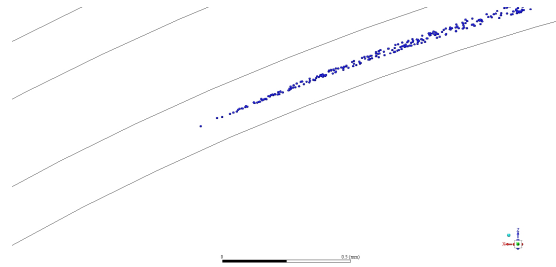


Figure 5.44: particles at 1° loop

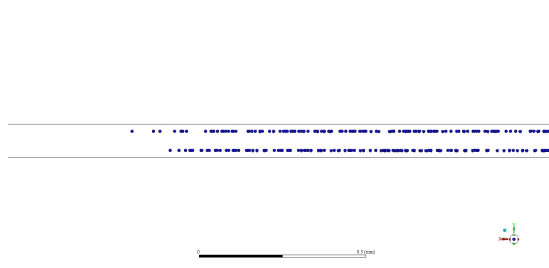


Figure 5.45: particles at 1° loop side view

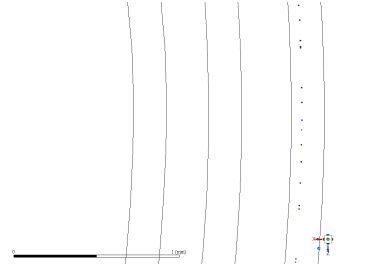


Figure 5.46: particles at 3° loop

As can be seen, the particles are focused at the inner wall and the distance of the particles is larger respect the previous simulation.

The particle to particle distance vary from 87 to $105\mu m$.

Chapter 6

FABRICATION OF THE SPIRAL CHANNEL

The spiral channel was fabricated in PMMA (Polymethyl methacrylate) also called Plexiglas. Using a vertical micro-milling machine engraved in a PMMA plate with dimensions of $30 \times 30 \times 1 \text{ mm}$ and covered with another flat PMMA plate of dimension $30 \times 30 \times 2.5 \text{ mm}$ holding inlet and outlet holes.

The software FUSION 360 was used with the CAD file, obtaining the CAM file (G-CODE) compatible with CNC machine as output.

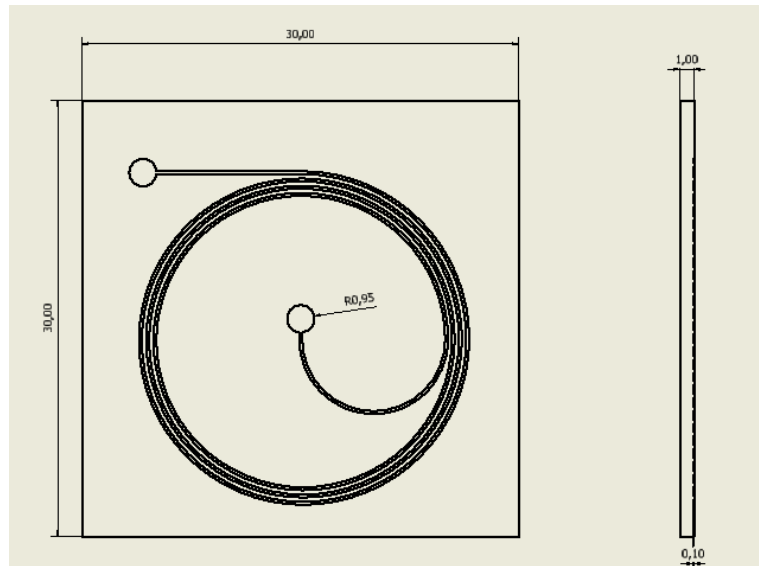


Figure 6.1: CAD drawing of the spiral in a plate of $30 \times 30 \text{ mm}$

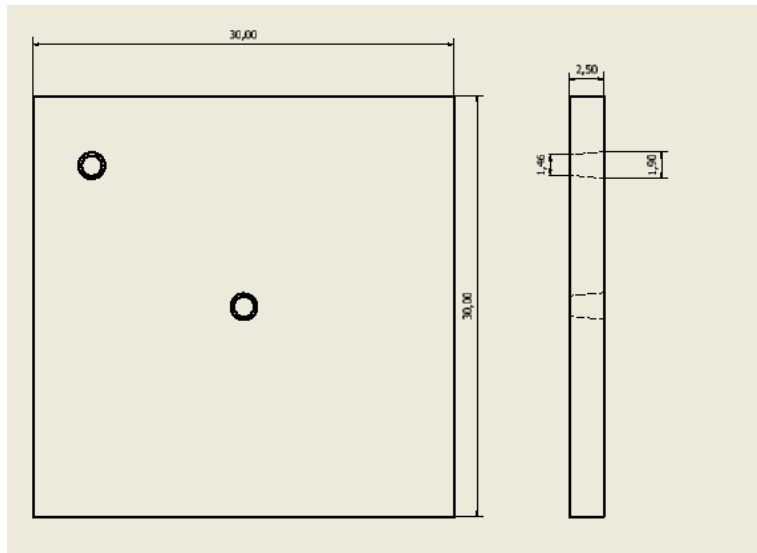


Figure 6.2: CAD drawing of the cover of the plate

Funnel-shaped holes were preferred with the aim to secure the capillary tubes and the stability of connections and avoid water leakage.

The outer diameter of the capillary tube used to deliver the liquid inside the spiral is 1.58 mm (inner diameter is 0.79 mm). Inlet holes were designed according to these dimensions.. Since the channel dimension is 200 μm , a 200 μm tip was used, requiring high speeds (20,000-26,000 rpm), low feeds (50 mm/min) and light passes (20-25 μm).

2 other spirals with different features were also realized and are reported in the following pictures:

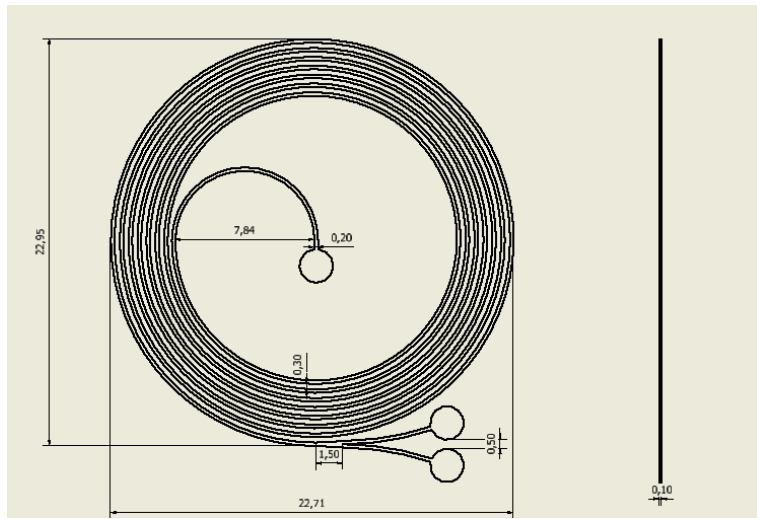


Figure 6.3: spiral geometry composed by seven loops

The first one has dimensions of 200x100 μm .

The other one is the same but is 200x50 μm .

An enlargement at the end of the spiral, before the outlet was made to be able to slow down the flow and a bifurcation to separate particles of different sizes.

The two PMMA plates, with spiral and holes respectively, were assembled in a clean room environment.

The procedure includes a washing step with IPA (isopropanol) and a thermal/solvent bonding with isopropanol heated to 70°C at low pressures in oven at 70°C (a paper sheet clamp was used to maintain the two plates aligned during heating). The isopropanol dissolves a small micro-layer of PMMA and therefore favours the bonding. The isopropanol must be hot to ensure that it evaporates and does not make the channels collapse.

The process to assemble the spiral device with 7 loops was difficult due to the high surface.

At the optical microscope inspection it was possible to see that the channels had collapsed and this did not allow the flow of liquid inside. For this reason, the spiral with 3 loops was selected for the following experiments.

Optical microscope was also used to check if the milling process was correct and to calculate the distance between channels or width of the channel as can be seen in Figure 6.4 and 6.5.

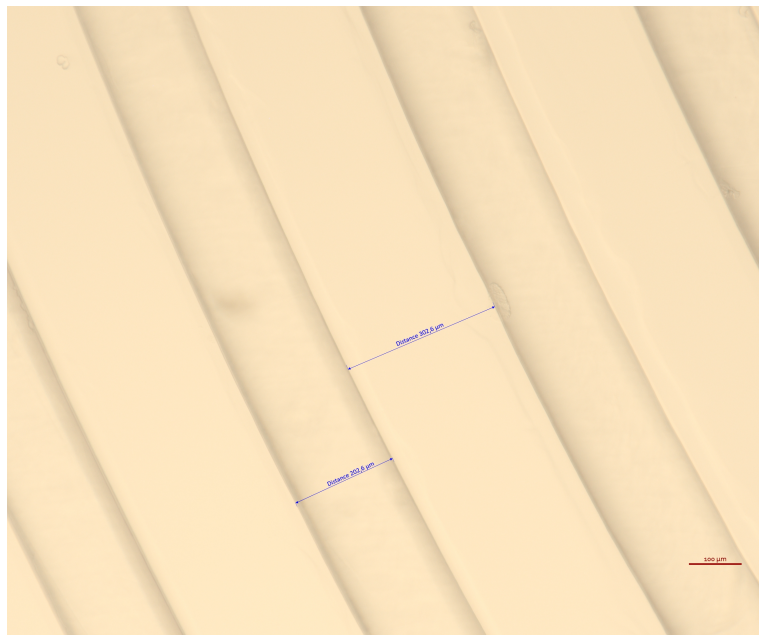


Figure 6.4: checking of the correct dimension of the spiral using a microscopy

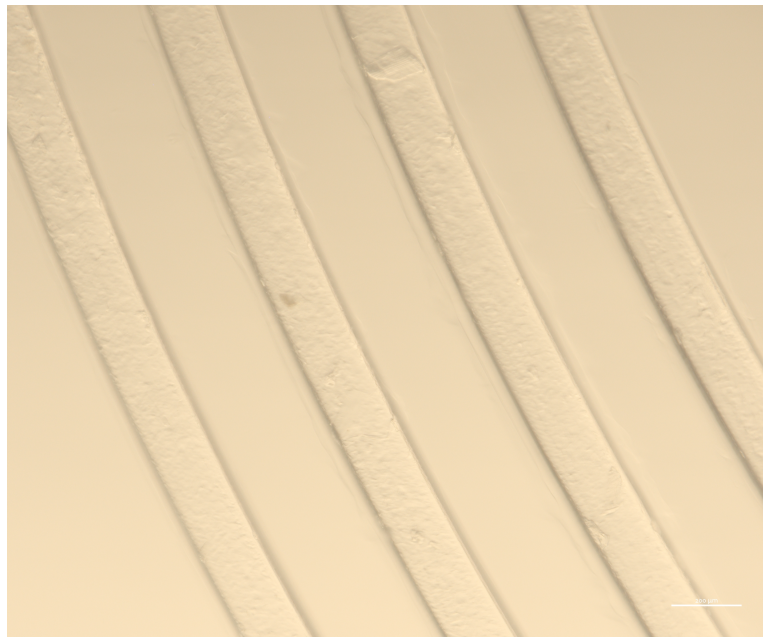


Figure 6.5: 3 loops looked at the microscopy

Chapter 7

EXPERIMENT SET UP AND FINAL RESULTS

7.1 Elveflow controller

In microfluidics systems, flows are generally laminar and due to the involved lenght-scale, gravity effects become negligible.

There are several ways to move a liquid in microfluidic system:

- 1)peristaltic pump
- 2)syringe pump
- 3)pressure driven flow controller

In this thesis last method was used.

ELVEFLOW controller is a microfluidic system in which it is possible to set pressure or flow rate.

The Elveflow micro pumping system (Elvesys, France) that was used is equipped with an OB1 base module. The Elveflow microfluidic flow controller OBI MK3+ allows the control of output pressure of up to 4 channels independently, from *-900 mbar* to *8 bar*, in five ranges:

- 1) 0 to 200 *mbar*;
- 2) 0 to 2000 *mbar*;
- 3) 0 to 8000 *mbar*;
- 4) -900 to 1000 *mbar*;
- 5) -900 to 6000 *mbar*

It is monitored by a computer through an interfacing device using the ESI software that allows

to perform real-time creation, monitoring and modifications on pressure profiles such as sine, square, triangle, ramp, pulse or sawtooth. The outport of Elveflow is connected to a reservoir with a large tube, while reservoir exit is connected to a microfluidic chip by a smaller tube (outer diameter of 1.58mm and inner diameter of 0.79mm). The system can read a negative and a positive pressure . A positive value indicates that the fluid is flowing from the reservoir to the microfluid chip, and a negative value indicates flow in the opposite direction.

The entire microfluidic setup, is shown in Figure 7.1. The microfluidic chip have been connected to the pump (channel 1 and 2, in Figure 7.1) to control the inlet pressure of the system, the inlets to the reservoirs containing the incoming fluids and their outlets represent the inlet capillaries of the chip. The device is positioned under a microscope with a mounted camera where the droplet generation can be observed and recorded.



Figure 7.1: setting of the experiment using ELVEFLOW controller

7.2 Injection of particles into the spiral and results

To validate the spiral design, Jurkat T lymphocyte cells were used in the experimental setup. Cells were labelled with DAPI. DAPI is a blue-fluorescent DNA staining dye, widely used to detect nuclei, and, when illuminated with precise wavelength excitation energy, higher wavelength light is emitted. In fluorescence molecules, electrons are able to move and the light excites these electrons bringing them to a higher energy state; when they return back to the minimum of energy they emit at a different length (higher than excitation one). Axio Zoom V16 fluorescence microscope (Zeiss, Oberkochen, Germany) with an Apo Z1x objective was used to detect cells. Around 640.000 cells were dispersed in a solution of $200 \mu\text{l}$ of PBS to preserve their integrity solutions with 1 ml volume were collected. It is possible to apply a simple calculation:

$$X = \frac{200 \cdot \text{CONCENTRATION}}{640000} \quad (7.1)$$

$$Y = 1000 - X \quad (7.2)$$

Where X is the volume of solution extract from the eppendorf that contains 640000 cells to obtain a CONCENTRATION (number of cells) inside a 1 *ml* of solution. Y is the PBS to add the the X solution to reach 1 *ml*.

In the following experiment concentration of 100.000 cells in 1 *ml* was used, setting a pressure of 1400 *mbar*.

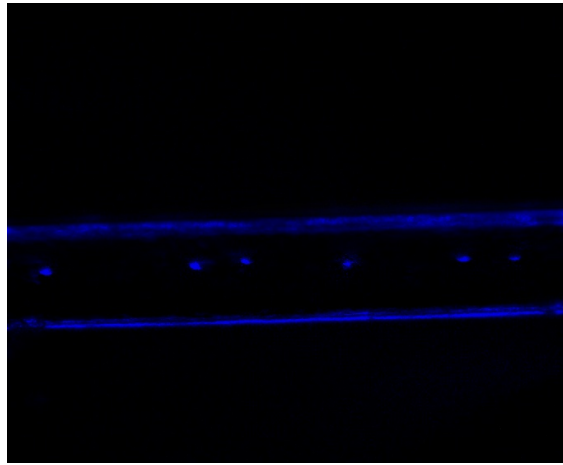


Figure 7.2: experiment picture of focusing particles at last loop

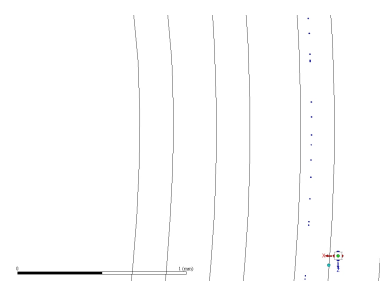


Figure 7.3: simulation result and focusing particles at last loop

Chapter 8

CONCLUSIONS

In the present work, a microfluidic device with spiral geometry was realized. The aim of the work was to identify a geometry and device features which can be useful to achieve an efficient particles separation. This is a very important aspect dealing with biological samples in general and blood in particular. In the case of the set-up of a CAR-T immunotherapy, for example, it is necessary to collect and count T cells, that are suspended in the blood in a disordered way and therefore the focusing and the alignment of the particle is necessary so that the sensor can count them.

The design process has required: the optimization of the cross section shape, number of loops, cross section size, space between loops, velocity of injection of particles and dimension of the spiral; the simulation of the spiral using ANSYS FLUENT improved with a UDF optimizing the mesh size to have a less computational time; the microfabrication of the spiral looking for the best setting of the micro-milling process.

To simulate the flow through a microfluidic channel by using the software ANSYS FLUENT, a UDF is needed in order to include the relevant microfluidic effects, namely the lift forces, which are not included in the basic software.

The results obtained in the simulation are consistent with the results observed in the experiments and this confirms the accuracy of the developed UDF.

In conclusion, the focusing of the particles can be achieved by designing a spiral that has a minimum of 3 loops to ensure the perfect alignment and spacing of the particles, a rectangular cross section of dimension $200 \times 100 \mu\text{m}$, a total dimension of the spiral of $22 \times 22 \text{ mm}$ and an injecting velocity of 0.75 m/s .

The possibility to separate a heterogeneous clinical sample in an automated way is important in the improvement of Lab on Chip for clinical purposes, also in the case of other applications different from the isolation of T Lymphocytes as described in this thesis work.

As it was seen in this thesis, the most critical part in the simulation is the implementation of a UDF to include the net lift force. The lift models were obtained from experimental data on rectangular section channels. One of the improvements may be to find a single model of the lift coefficient valid

for all types of cross section, in which it is a step forward in fluid dynamics simulation but also in microfluidics. Another improvement can be to simulate the particles considering them as solid and deformable bodies and not as points as FLUENT does, in this way it is also possible to insert repulsion forces between the particles that allow a simulation closer to reality.

Bibliography

- [1] Amini, H., Lee, W., Carlo, D. D. (2014). Inertial microfluidic physics. *Lab on a Chip*, 14(15), 2739–2761
- [2] J. F. Richardson, J. M. Coulson, J. Harker and J. Backhurst, *Chemical Engineering: Particle technology and separation processes*, Butterworth-Heinemann, 2002
- [3] E. Michaelides, *Particles, bubbles drops: their motion, heat and mass transfer*, World Scientific, Singapore, 2006
- [4] S. Rubinow and J. B. Keller, *J. Fluid Mech.*, 1961, 11, 447-459
- [5] E. S. ASMOLOV, *J. Fluid Mech.*, 1999, 381, 63-87
- [6] J. Zhou and I. Papautsky, *Lab Chip*, 2013, 13, 1121-1132
- [7] D. Di Carlo, D. Irimia, R. G. Tompkins and M. Toner, *Proc. Natl. Acad. Sci. U.S.A.*, 2007, 104, 18892–18897
- [8] D. Di Carlo, J. F. Edd, K. J. Humphry, H. A. Stone and M. Toner, *Phys. Rev. Lett.*, 2009, 102, 94503
- [9] Dean W. R. LXXII. The stream-line motion of fluid in a curved pipe (Second paper). *The London, Edinburgh, and Dublin Philosophical Magazine and Journal of Science* 5, 673–695 (1928)
- [10] A. A. S. Bhagat, S. S. Kuntaegowdanahalli, N. Kaval, C. J. Seliskar and I. Papautsky, *Biomed. Microdevices*, 2010, 12, 187-195
- [11] Bhagat A. A. S., Kuntaegowdanahalli S. S., and Papautsky I., *Phys. Fluids* 20, 101702 (2008).[10.1063/1.2998844](https://doi.org/10.1063/1.2998844)
- [12] Chun B. and Ladd A. J. C., *Phys. Fluids* 18, 031704 (2006).[10.1063/1.2176587](https://doi.org/10.1063/1.2176587)
- [13] Zhou J., Giridhar P. V., Kasper S., and Papautsky I., *Lab Chip* 13, 1919–1929 (2013).[10.1039/c3lc50101a](https://doi.org/10.1039/c3lc50101a)
- [14] Spiral microchannel with rectangular and trapezoidal cross-sections for size based particle separation Guofeng Guan, Lidan Wu, Ali Asgar Bhagat, Zirui Li, Peter C. Y. Chen, Shuzhe Chao, Chong Jin Ong Jongyoon Han

- [15] G. Segre, Nature, 1961, 189, 209-210
- [16] Single stream inertial focusing in low aspect-ratio triangular microchannels Prithviraj Mukherjee,a Xiao Wang,b Jian Zhou a and Ian Papautsky
- [17] Yang, B. H. et al. Migration of a sphere in tube flow. Journal of Fluid Mechanicsb 540, 109–131 (2005).
- [18] Prohm, C., Gierlak, M. Stark, H. Inertial microfluidics with multi-particlebcollision dynamics. The European physical journal. E, Soft matter 35, 9757 (2012).
- [19] L. Sprenger, S. Dutz, T. Schneider, S. Odenbach, and U. O. Hafeli, “Simulation and experimental determination of the online separation of blood components with the help of microfluidic cascading spirals,” Biomicrofluidics 9, 044110 (2015).
- [20] S. Dutz, M. E. Hayden, A. Schaap, B. Stoeber, and U. O. Hafeli, “A microfluidic spiral for size-dependent fractionation of magnetic microspheres,” J. Magn. Magn. Mater. 324, 3791 (2012)

Appendix A

```
/* UDF adding an external body force to the particles */
#include "udf.h"
#include "mem.h" /* cell indexing header */
#include "dpm.h"
/* particle properties even though declared in the macro arguments */
/* #include "metric.h" */
/*#include <math.h> */

DEFINE_DPM_BODY_FORCE(particle_body_force ,p, i)
{
/* declaration of variables */
double w, Dh, Ufx, Ufy, Ufz, Gx, rho, a, F_L, c_height, c_length,
c_volume, side, H, W, f_height_total, Renx, Reny, Renz, crDh, mu,
aUfx, aUfy, aUfz, C1, C2, C3, C4, C_Ly, C_Lz, z, y;

cell_t c = P_CELL(p);
/* the cell initialization in which the particle is present*/
Thread *t = P_CELL_THREAD(p); /* thread initialization */
c_volume = C_VOLUME(c , t); /*volume of th cell mesh that can varay */

c_height = 0.001; /* mesh cell sizes in cross section*/
c_length = 0.002; /* mesh cell sizes in cross section*/
side = c_volume/(c_height*c_length);
/* calculating the lenght of the cell in the channel */
H = 0.00005; /*height of the cross section of the channel */
W = 0.0001; /*width of the cross section of the channel */
```

```

Dh = 0.00006667; /*hydraulic diameter of the channel */
mu = 0.001003; /*viscosity of the fluid */
rho = C_R(c, t);
Ufx = C_U(c, t);
Ufy = C_V(c, t);
Ufz = C_W(c, t);
aUfx = fabs(Ufx); /* absolute value of Ufx */
aUfy = fabs(Ufy); /* absolute value of Ufy */
aUfz = fabs(Ufz); /* absolute value of Ufz */

/* local Reynolds number calculation*/

Renx = (rho*aUfx*Dh)/mu;
Reny = (rho*aUfy*Dh)/mu;
Renz = (rho*aUfz*Dh)/mu;

/*lift force calculation*/

z=(fabs(P_POS(p)[2])/(H/2));
y=(fabs(P_POS(p)[1])/(H/2));

Gx = (2*0.2667)/H; /*max shear rate of the channel*/

a = P_DIAM(p); /* particle diameter */

C1=-3.0374;
C2=-0.3046;
C3= 0.9790;
C4=-0.0016;

/*value of C_L for 2y/H */
C_Ly =C1*pow(y,3)+C2*pow(y,2)+C3*pow(y,1)+C4*pow(y,0);

if (z>=0 && z<=1.2)
{
C_Lz =((0.047-y*(0.077/0.6))/1.2)*z;
}
else if (z>1.2)

```

```

{
/*value of C_L for 2z/H */
C_Lz =(7.3046*((y*(0.077/0.6))-0.127)*pow(z,2) +
-17.531*((y*(0.077/0.6))-0.127)*z+9.51863*((y*(0.077/0.6))-0.135405));
}

/*calculate sign*/

if ( i==1)
{
if (P_POS(p)[1]>=0)
{
F_L= rho*pow(Gx,2)*pow(a,4)*C_Ly;
}
}

else
{
F_L= -rho*pow(Gx,2)*pow(a,4)*C_Ly;
}

if ( i==2)
{
if (P_POS(p)[2]>=0)
{
F_L= rho*pow(Gx,2)*pow(a,4)*C_Lz;
}
else
{
F_L= -rho*pow(Gx,2)*pow(a,4)*C_Lz;
}

if ( i==0)
{
F_L=0;
}
}

```

```
return (F_L/P_MASS(p));  
}  
  
//it is very important to put all condition along  
the 3 axis i=0,1,2 because if you miss one  
//FLUENT will give a value that it wants and you can have  
a different trajectory and problem of escaped particles. //
```

Appendix B

```
/* UDF adding an external body force to the particles */
#include "udf.h"
#include "dpm.h"
#include "dpm_mem.h"
#include "surf.h"
#include "metric.h"

DEFINE_DPM_BODY_FORCE(particle_body_force , p, i)
{

/* declaration of variables */
double Dh, Ufx, Ufy, Ufz, Gx, rho, a, F_L, c_height, c_length,
c_volume, side, f_height_total, Renx, Reny, Renz, crDh, mu, aUfx,
aUfy, aUfz, C1, C2, C3, C4, C_Ly, C_Lz, z, y,H,W;

real xw[ND_ND]; //centroid vector
real vec[ND_ND];
Domain* d; //domain d that for one phase(only water) is always 1
cell_t c; //cell of the thread t
Thread* t;
face_t f;
//f is the face index that is inside the face thread t(our wall).
//You will extract the face area vector from f index
d = Get_Domain(1);
c = P_CELL(p); //cell in which the particle is currently in
t = Lookup_Thread(d, 9); //9 is the ID number of the upper wall.
//t is the thread index(pointer) of the wall boundary surface 9
```

```

//int count=0;
real distancewally = 100.0; //initial random setting to do comparison
int fid = 0; //initial setting
real vector [ND_ND];
begin_f_loop(f, t)
{
    F_CENTROID(xw, f, t); //center of each face
    NV_VV(vec, =, xw, -, P_POS(p));
    //vector connecting the particle to the face center that is placed
    //at the wall. The NV_VV do the operation between
    //2 vectors :(vec=xw-P_POS(p))

    if (distancewally >= NV_MAG(vec))
        //in this way i found the min distance but is not ortoginal to the wall
    {
        distancewally = NV_MAG(vec);
        fid = f;
        vector [0] = vec [0];
        vector [1] = vec [1];
        vector [2] = vec [2];
    }
    // count = count + 1;
    // Message("count is:%d\n", count);

}
end_f_loop(f, t)
//Message("fid is:%d\n", fid);

real A[ND_ND];
real AMag;

F_AREA(A, fid, t);
//unit normal vector of the face with id f in the thread t with id 9

```

```

AMag = NV_MAG(A); //magnitude of the vector A
A[0] = A[0] / AMag;
A[1] = A[1] / AMag;
A[2] = A[2] / AMag;
distancewally = NV_DOT(vector , A);
//distance wall , you do the dot product(projection)

// Message("NX:%g\n", A[0]);
// Message("NY:%g\n", A[1]);
// Message("NZ:%g\n", A[2]);
// Message("AMag:%g\n", AMag);
//Message("walldist y: %g\n", distancewally);

Thread* tt = P_CELL_THREAD(p);

H = 0.0001; /*height of the cross section of the channel */
W = 0.0002; /*width of the cross section of the channel */
// Dh = 0.00006667; /*hydraulic diameter of the channel */
mu = 0.001003; /*viscosity of the fluid */
rho = C_R(c, tt);
Ufx = C_U(c, tt);
Ufy = C_V(c, tt);
Ufz = C_W(c, tt);
aUfx = fabs(Ufx); /* absolute value of Ufx */
aUfy = fabs(Ufy); /* absolute value of Ufy */
aUfz = fabs(Ufz); /* absolute value of Ufz */

/* local Reynolds number calculation*/

Renx = (rho * aUfx * Dh) / mu;
Reny = (rho * aUfy * Dh) / mu;
Renz = (rho * aUfz * Dh) / mu;

Gx = (0.375*2) / H; /*max shear rate of the channel*/
a = P_DIAM(p); /* particle diameter */

y = fabs(((H / 2) - distancewally) / (H / 2));

```

```

double    p00, p10, p01, p20, p11, p02, p30, p21, p12, p03, p40,
p31, p22, p13, p04, p50, p41, p32, p23, p14, p05;

/*valori dei coefficienti del polinomio CLy*/
p00 = -0.001042;
p10 = 0.8902;
p01 = -0.01908;
p20 = 0.8614;
p11 = -0.1395;
p02 = 0.03062;
p30 = -8.634;
p21 = 1.774;
p12 = -0.6554;
p03 = 0.05971;
p40 = 12.58;
p31 = -2.311;
p22 = -0.6657;
p13 = 0.445;
p04 = -0.09484;
p50 = -8.44;
p41 = 0.3353;
p32 = 1.863;
p23 = -0.04633;
p14 = -0.1522;
p05 = 0.03128;

t = Lookup_Thread(d, 7);

real distancewallzx = 100.0; //i'm setting an generic initial value
int fidd = 0;
real vettore[ND_ND];
// real ppos[ND_ND] = P_POS(p);

begin_f_loop(f, t)
{
    F_CENTROID(xw, f, t); //center of each face
    NV_VV(vec, =, xw, -, P_POS(p));
}

```

```

//vector connecting the particle to the face center that is
//placed at the wall. The NV_VV do the operation between
//2 vectors :( vec=xw-P_POS(p))

//now you want to calculate the minimum distance between particle
//and wall , and so you want to find the minimum of the vector vec
//doing the loop over all the boundary face

if ( distancewallzx >= NV_MAG( vec ) )
{
    distancewallzx = NV_MAG( vec );
    fidd = f;
    vettore [0] = vec [0];
    vettore [1] = vec [1];
    vettore [2] = vec [2];
}

end_f_loop(f, t)

real AA[ND_ND];
real AAMag;

F_AREA(AA, fidd, t);
//unit normal vector of the face with id f in the thread t with id 9
AAMag = NV_MAG(AA);
AA[0] = AA[0] / AAMag;
AA[1] = AA[1] / AAMag;
AA[2] = AA[2] / AAMag;
distancewallzx = NV_DOT(vettore, AA); //distance wall

// Message("walldist zx: %g\n", distancewallzx );
//Message("A_Z:%g\n", AA[2]);
// Message("A_X:%g\n", AA[0]);
//Message("sono all 'ID:%d\n", THREAD_ID(t));

```

```

z = fabs((W / 2) - distancewallzx) / (H / 2));

C_Ly = p00 + p10 * y + p01 * z + p20 * pow(y, 2) + p11 * y * z +
p02 * pow(z, 2) + p30 * pow(y, 3) + p21 * pow(y, 2) * z +
p12 * y * pow(z, 2) + p03 * pow(z, 3) + p40 * pow(y, 4) +
p31 * pow(y, 3) * z + p22 * pow(y, 2) * pow(z, 2) + p13 * y * pow(z, 3) +
p04 * pow(z, 4) + p50 * pow(y, 5) + p41 * pow(y, 4) * z +
p32 * pow(y, 3) * pow(z, 2) + p23 * pow(y, 2) * pow(z, 3) +
p14 * y * pow(z, 4) + p05 * pow(z, 5);

real C_Lyy[ND_ND];

if (C_Ly >= 0)
{
    C_Lyy[1] = C_Ly* A[1];
}
else
{
    C_Lyy[1] = fabs(C_Ly) * (-A[1]);
}

if (i == 1)
{
    if (distancewally <= H / 2)
    {
        F_L = rho * pow(Gx, 2) * pow(a, 4) * C_Lyy[1];
    }
    else if (distancewally > H / 2)
    {
        F_L = -(rho * pow(Gx, 2) * pow(a, 4) * C_Lyy[1]);
    }
    // Message("Fy is:%g\n", F_L);
    /* FILE* pffy;
    if (NULL == (pffy = fopen("Fy.txt", "a")))
        Error("Could not open file for append!\n");
    fprintf(pffy, "%e %g\n", F_L, CURRENT_TIME);
    fclose(pffy); */
}

```

}

```
/*valori dei coefficienti del polinomio CLz*/
p00 = -0.009432;
p10 = 0.07128;
p01 = 0.1484;
p20 = 0.6319;
p11 = -1.232;
p02 = -0.3231;
p30 = -1.838;
p21 = 2.89;
p12 = 0.5397;
p03 = -0.7474;
p40 = 1.78;
p31 = -2.553;
p22 = -1.325;
p13 = -0.04154;
p04 = 2.891;
p50 = -0.5609;
p41 = 0.7351;
p32 = 0.8185;
p23 = -0.5963;
p14 = 0.5391;
p05 = -2.159;

C_Lz = p00 + p10 * z + p01 * y + p20 * pow(z, 2) + p11 * z * y +
p02 * pow(y, 2) + p30 * pow(z, 3) + p21 * pow(z, 2) * y +
p12 * z * pow(y, 2) + p03 * pow(y, 3) + p40 * pow(z, 4) +
p31 * pow(z, 3) * y + p22 * pow(z, 2) * pow(y, 2) +
p13 * z * pow(y, 3) + p04 * pow(y, 4) + p50 * pow(z, 5) +
p41 * pow(z, 4) * y + p32 * pow(z, 3) * pow(y, 2) +
p23 * pow(z, 2) * pow(y, 3) + p14 * z * pow(y, 4) + p05 * pow(y, 5);

// Message("y: %g\n", y);
```

```

// Message("CLZ is:%g\n", C_Lz);

real C_Lzz[ND_ND];

if (C_Lz >= 0)
{
    C_Lzz[0] = C_Lz * (AA[0]);
    C_Lzz[2] = C_Lz * (AA[2]);
}
else
{
    C_Lzz[0] = fabs(C_Lz) * (-AA[0]);
    C_Lzz[2] = fabs(C_Lz) * (-AA[2]);
}

// for (i = 0; i <= 2; i = i + 1)
// {

if (i == 2)
{
    if (distancewallzx <= W / 2)
    {
        F_L = (rho * pow(Gx, 2) * pow(a, 4) * C_Lzz[2]);
    }
    else
    {
        F_L = -(rho * pow(Gx, 2) * pow(a, 4) * C_Lzz[2]);
    }
    // Message("Fz is:%g\n", F_L);
    /*FILE* pffz;
    if (NULL == (pffz = fopen("Fz.txt", "a")))
        Error("Could not open file for append!\n");
    fprintf(pffz, "%e %g\n", F_L, CURRENT_TIME);
    fclose(pffz);*/
}
}

```

```

    if ( i == 0)
    {

        if ( distancewallzx <= W / 2)
        {
            F_L = ( rho * pow(Gx, 2) * pow(a, 4) * C_Lzz[0]);
        }
        else
        {
            F_L = -(rho * pow(Gx, 2) * pow(a, 4) * C_Lzz[0]);
        }

        // Message("Fx is:%g\n", F_L);

        /*FILE* pffx ;
        if (NULL == (pffx = fopen("Fx.txt", "a")))
            Error("Could not open file for append!\n");

        fprintf(pffx , "%e %g\n",F_L, CURRENT_TIME);
        fclose(pffx);*/
    }

    // }

//Message("i1 mio ID :%d\n",myid);
// Message("tempo:%g\n", CURRENT_TIME);
//real current flow time
// Message("iteration fluid:%d\n", N_ITER);
//integer number of iteration of fluid

//you will plot the message every DPM iteration(that is 10)
even if the computer calculate the others steps
// Message("x position:%g\n", P_POS(p)[0]);
// Message("y position:%g\n", P_POS(p)[1]);
// Message("z position:%g\n", P_POS(p)[2]);

int time_steps;
int iter;
time_steps = N_TIME;

```

```

iter = N_ITER;

/* FILE* pf;
if (NULL == (pf = fopen("C_Lz.txt", "a")))
    Error("Could not open file for append!\n");

fprintf(pf, "%e %e %d %g %e %e \n", C_Lz, z, time_steps,
        iter, CURRENT_TIME, distancewallzx, distancewally);

fclose(pf);

FILE* pff;
if (NULL == (pff = fopen("C_Ly.txt", "a")))
    Error("Could not open file for append!\n");

fprintf(pff, "%e %e %g\n", C_Ly, y, CURRENT_TIME);
fclose(pff);
*/



return (F_L / P_MASS(p));
}

```